10-5-2017

A Multi-Sensor Platform for Microcurrent Skin Stimulation during Slow Wave Sleep

Francia Dauz
University of Windsor

A Multi-Sensor Platform for Microcurrent Skin Stimulation during Slow Wave Sleep

By

Francia Tephanie Dauz

A Thesis
Submitted to the Faculty of Graduate Studies
through the Department of Electrical and Computer Engineering
in Partial Fulfillment of the Requirements for
the Degree of Master of Applied Science
at the University of Windsor

Windsor, Ontario, Canada

2017

A Multi-Sensor Platform for Microcurrent Skin Stimulation during Slow Wave Sleep

By

Francia Tephanie Dauz

Approved By:

_____

W. Kedzierski

Department of Physics

_____

M. Ahmadi

Department of Electrical and Computer Engineering

_____

R. Maev, Advisor

Department of Electrical and Computer Engineering

September 13th, 2017

Declaration of Originality

I hereby certify that I am the sole author of this thesis and that no part of this thesis has been published or submitted for publication.

I certify that, to the best of my knowledge, my thesis does not infringe upon anyone's copyright nor violate any proprietary rights and that any ideas, techniques, quotations, or any other material from the work of other people included in my thesis, published or otherwise, are fully acknowledged in accordance with the standard referencing practices. Furthermore, to the extent that I have included copyrighted material that surpasses the bounds of fair dealing within the meaning of the Canada Copyright Act, I certify that I have obtained a written permission from the copyright owner(s) to include such material(s) in my thesis and have included copies of such copyright clearances to my appendix.

I declare that this is a true copy of my thesis, including any final revisions, as approved by my thesis committee and the Graduate Studies office, and that this thesis has not been submitted for a higher degree to any other University or Institution.

Abstract

Insufficient and low quality sleep is related to several health issues and social outcomes. Regular sleep study conducted in a sleep laboratory is impractical and expensive. As a result, miniature and non-invasive sleep monitoring devices provide an accessible sleep data. Though not as accurate as polysomnography, these devices provide useful data to the subject by tracking sleep patterns regularly. On the other hand, proactive improvement of sleep quality has been limited to pharmacological solutions and cranial electrotherapy stimulation. An alternative approach and a potential solution to sleep deprivation is a non-pharmacological technique which involves the application of micro-current electrical stimulation on the palm during Slow Wave Sleep (SWS). This thesis presents the development of a miniature device for SWS detection and electrocutaneous stimulation.

Several sensors are embedded in the prototype device to measure physiological data such as body movement, electrodermal activity, heart rate, and skin and ambient temperature. Furthermore, the prototype device provides local storage and wireless transfer for data acquisition. The quality of the sensor data during sleep are discussed in this thesis. For future work, the results of this thesis shall be the used as a baseline to develop a more refined prototype for clinical trials in sleep laboratories.

I dedicate my thesis to my family and friends who supported me along the way.

Acknowledgements

My sincerest gratitude to my supervisor, Dr. Roman Maev, for his continuous support throughout the span of this research. I would also like to thank Dr. Emil Strumban, Dr. Alex Denisov, Serge Zhelkanov and Alex Lyadski for sharing their knowledge and expert advice during the development of this project.

I also appreciate the time and guidance of my committee members, Dr. Majid Ahmadi and Dr. Wladyslav Kedzierski.

Contents

List of Tables

List of Figures

Abbreviations

API	**A**pplication **P**rogram **I**nterface
ADC	**A**nalog-to- **D**igital **C**onverter
CES	**C**ranial **E**lectrotherapy **S**timulation
DC	**D**irect **C**urrent
ECG	**E**lectro**C**ardio **G**ram
EDA	**E**lectro**D**ermal **A**ctivity
EEG	**E**lectro**E**ncephalo **G**raphy
EMG	**E**lectro**M**yo **G**raphy
HAL	**H**ardware **A**bstraction **L**ayer
FAT	**F**ile **A**llocation **T**able
FIFO	**F**irst **I**n **F**irst **O**ut
IC	**I**ntegrated **C**ircuit
MCU	**M**icro**C**ontroller **U**nit
PPG	**P**hoto**P**lethysmo **G**raphy
PSG	**P**oly**S**omno **G**raphy
REM	**R**apid**E**ye **M**ovement
RISC	**R**educed Instruction Set Computing
RTOS	**R**eal- **T**ine **O**perating **S**ystem
SWS	**S**low **W**ave **S**leep

Chapter 1

Introduction

Sleep deprivation has been found to be related to a wide range of health issues such as stress, cognitive performance degradation and fatigue. A study from RAND company in 2016 reported that around $418 billion$ is lost in workplace productivity due to sleep deprived workers[1]. It was also reported that individuals who sleep less than 6 hours per night have 10% higher mortality risk. Thus, there is a significant demand to improve sleep quality in the general public by providing affordable sleep aid devices.

1.1 Motivation

Polysomnography (PSG) is the traditional method of monitoring sleep by recording bioelectrical signals using electroencephalography (EEG), electro-oculogram (EOG), electrocardiogram (ECG), and electromyogram (EMG) [2]. The characteristics of these physiological signals correspond to specific sleep stage. It is well established that sleep is divided into two main stages: Rapid Eye Movement (REM) and Non-Rapid Eye Movement (NREM). NREM is further divided into four stages (Stage 1, Stage 2, Stage 3 and Stage 4); however, Stage 3 and Stage 4 are later combined into one stage N3 [3] . N3 stage is also referred to as Slow Wave Sleep SWS for the presence of delta waves which are characterized by a high

spectral power of synchronized low frequency oscillations in the range of 0.5 to 4 Hz [4].

The importance of SWS has been explored by researchers and was shown to be related to cerebral restoration and recovery[5], mediation of learning and declarative memory processing[6], regulation of homeostasis of sleep, secretion of growth hormone, and reduction of daytime sleepiness and fatigue. Due to these benefits of SWS, methods in enhancing SWS stage of sleep have also been studied. Pharmacological, where hypnotic drugs are taken, and Cranial Electrotherapy stimulation, pulsed low-intensity electrical currents are applied to the scalp, are examples of methods inducing SWS. However, negative side effects are unclear with long term intake of pharmacological drugs and direct electrostimulation of the braid [7]. A successful study in increasing SWS was performed where in a subthreshold electrocutaneous skin stimulation was applied to palm skin[8] . With this motivation, a multi-sensor platform for detecting SWS and applying stimulation is developed.

1.2 Problem Statement

The objective of this research thesis is to design a portable sleep monitoring device that identifies Slow Wave Sleep(SWS) and provide electrocutaneous stimulation on the palm skin.

1.3 Thesis Contribution and Limitation

The scope of this thesis is the design and implementation of a wireless wearable device for slow wave sleep detection and application of sub-threshold electrical stimulation during SWS. The device prototype will be used to collect data during sleep to determine when the subject is in deep sleep stage and provide low current stimulation on the palmar surface. A series of hardware designs are presented in this thesis which ultimately leads to a single design chosen to satisfy the requirements of this project. This thesis focuses on the development of the device

and does not extend to the analysis of the effectiveness of the electrocutaneous stimulation to increase the slow wave sleep stage.

1.4   Research Publication

F. Dauz, E. Strumban and R. G. Maev, "Wearable device for increasing the slow wave sleep stage by electrocutaneous stimulation," 2017 IEEE 30th Canadian Conference on Electrical and Computer Engineering (CCECE), Windsor, ON, 2017, pp. 1-3. ©2017 IEEE

1.5   Thesis Outline

This thesis is divided into five chapters. The first chapter introduces the overall composition of the project and the motivation behind the development of the prototype device. Chapter 2 focuses on the background study of the architecture of sleep and several sleep aid devices. It presents several methods of monitoring sleep and enhancing sleep quality. Next, Chapter 3 focuses about the design requirements and process. The two parts of the prototype device development are hardware and software/firmware. Chapter 3 also explores the available technical solutions and the rationale of the chosen design. The results of evaluating the performance of the chosen design and discussion are written in Chapter 4. Lastly, Chapter 5 summarizes the conclusion and future scope of the project.

Chapter 2

Background and Literature Review

Sleep monitoring is the method of quantifying sleep by translating physiological signals into several parameters such as total length of sleep, each sleep stage in the sleep cycle and amount wakefulness or sleep interruption. The integration of these parameters results to scoring the quality of one's sleep. Accurate and regular sleep monitoring helps diagnose sleep disorders such as insomnia and obstructive sleep apnea. Polysomnography as well as alternative sleep monitoring methods are introduced in this chapter. Various studies that investigated the correlation of a specific physiological signal with sleep and the corresponding results are also presented. In addition, this chapter explores several methods of enhancing the quality of sleep.

2.1   Sleep Staging Methods

2.1.1   Polysomnography

Polysomnography (PSG) is the traditional method of monitoring sleep by recording bioelectrical signals using electroencephalography (EEG), electro-oculogram (EOG), electrocardiogram (ECG), and electromyogram (EMG). A summary of the characteristics of the sleep stages using these physiological signals are shown in Table 2.1. Conventionally, sleep stages are classified using brainwave data collected using multi-channel EEG. Brainwaves are divided into five groups according to frequency range: delta wave (0-4Hz), theta wave (4-8Hz), alpha wave (8-12Hz), beta wave (12-30Hz) and gamma wave (>30 Hz) [9]. Currently, there are sleep monitoring devices available in the market that use much less number of EEG electrodes or channel. An example is the Zeo Sleep Manager and Sleep Profiler. Furthermore, an automated sleep classification using a single EEG channel has been studied in [10]. Radha et al. investigated the feature and the classifier algorithm that will give the most accurate sleep staging based on a single EEG signal. They have concluded that the signals from frontal channels lead to best classifying performance, and random forest gave better results compared to support vector machine (SVM) for the classification algorithm [11]. Wearable and portable EEG such as Brain-Computer Interface (BCI) devices also support the collection of brainwaves in sleep monitoring [12].

TABLE 2.1: Summary of Sleep Stage Characteristics[13]

Stage	EEG	EOG	EMG
Wake (eyes open)	Low-voltage, high-frequency, attenuated alpha activity	Eye blinks, REMs	Relatively High
Wake(eyes closed)	Low-voltage, high-frequency, >50% alpha activity	Slow-rolling eye movements	Relatively high
Stage 1	Low-amplitude, mixed-frequency, <50% alpha activity, no spindles, K complexes	Slow Rolling eye movements	May be lower than wake
Stage 2	At least one sleep spindle or K complex <20% slow-wave activity		May be lower than wake
Stage 3	>20% slow-wave activity	SWS seen in EOG	Usually low
REM	Low-voltage, mixed frequency, sawtooth waves may be present	Episodic REMs	Relatively reduces (equal or lower than the lowest in NREM)

PSG is performed in the sleep laboratory with the assistance of a sleep technician making it impractical for regular sleep monitoring. As a result, wearable devices or activity trackers such as Microsoft Band, JawBone 3, FitBit One which include sleep monitoring feature are gaining popularity. There are several advantages for these devices. First, they are portable and require no assistance from a professional. Second, they are comfortable and are not obstructive to the user during sleep. Lastly, the results of the overnight sleep is available immediately to the user, unlike PSG where a professional has to interpret the data recorded. For simplicity, researchers minimized the number of bioelectrical signal required to

accurately score sleep. A summary of the different approaches of portable sleep monitoring in determining SWS is shown in Table 2.2.

TABLE 2.2: Portable Sleep Monitoring Devices

Author	Design Feature	Comments
Sano et al, Liguori et al	Actigraphy, EDA & Skin temperature measurement	80% of EDA peaks found in SWS and NREM 2
Liang et al, Krike et al	Actigraphy	Sleep-wake identification only
Polat et al	Photophlethysmography	Significant changes in PPG signals between apnea and normal classes

2.1.2   Actigraphy

Another non-invasive method in determining sleep quality is by tracking the subject's movement overnight. Actigraphy is a method that uses accelerometer to detect movement which is mainly used in wrist-worn sleep monitoring devices. Actigraphy alone can be accurate to distinguish sleep-wake pattern, but could be improved if other parameters such as pulse oximeter or EEG is taken into consideration [14, 15]. Peng et al. also mentioned that actigraphy may fail to detect wakefulness for inactive sleepers [16]. A different approach in tracking movement during sleep is using image processing with data collected from a camera as proposed in [17] and [18]. In addition,a study proposed the use of mattress indentation measurement to analyze motor patterns during sleep and a pressure sensitive bedsheet to classify sleep between WAKE, REM, and NREM stages [19, 20].

2.1.3 Electrodermal Activity

Electrodermal activity (EDA) pattern is another physiological parameter that is used in sleep staging. EDA, also known as Galvanic Skin Response (GSR), is related to the synchronized activation of sweat glands as a response to sympathetic nervous system [21]. It has two main components: tonic and phasic. Tonic is the slow changing component which reflects general changes in autonomic arousal while phasic is fast changing and is also called Skin Conductance Response (SCR). More than 80% of EDA peaks was found in SWS and N2 stage, and EDA levels were higher when measured from the wrist compared to palm according to Sano et al. [22]. This result agrees with the findings of Liguori et al that EDA is more frequent in NREM 4 or SWS sleep stage [21]. Sleep period time was estimated using EDA and proved that EDA yields a more accurate result compared to actigraphy in estimating the total length of sleep[23]. The use of EDA pattern in developing an automated sleep monitor seems to be feasible. However, the challenges will be the effect of skin temperature and electrode contact with the skin over time. An example of an SCR event or EDA peak with its corresponding properties is shown in Figure 2.1.
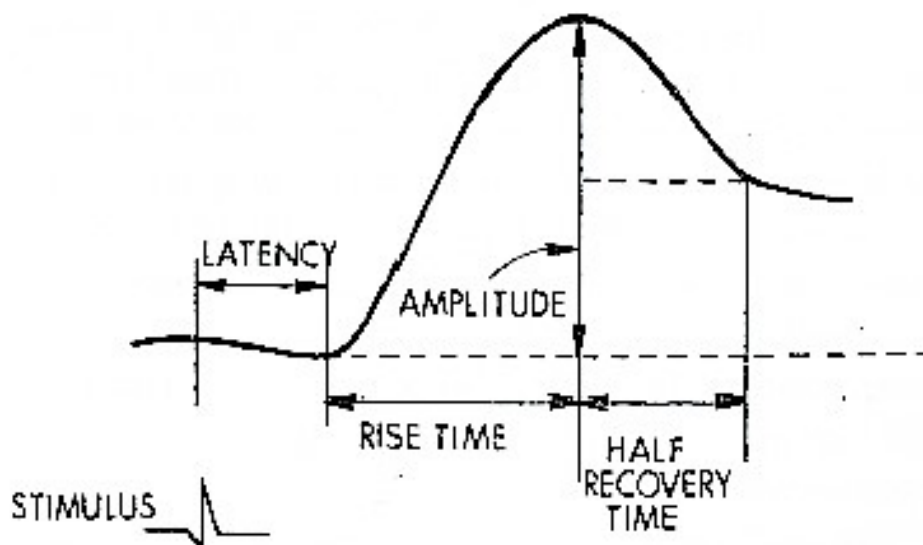
FIGURE 2.1: EDA signal components[24]

2.1.4 Electrocardiography

Several features can be extracted from ECG data and be used in sleep staging such as Heart Rate Variability (HRV) and R-R peak interval [25]. Cardiac activity could also be measured using photoplethysmography (PPG) method which uses reflective photosensors to measure pulse rate and blood flow[26]. Recent study also showed that PPG signals have significant changes between normal class and sleep apnea class during respiratory events[27]. These automated sleep monitoring devices implement different machine learning algorithms such as Hidden Markov Models (HMM) and decision tree based VSM [28–30]. One paper proposed a new algorithm in sleep classification using ECG signal and EMG but found a low agreement ratio result with PSG [31]. ECG data is usually collected by placing an electrode in each arm and a bias electrode known as the Right Leg Drive. On the other hand, a PPG sensor could be placed on the fingers or the wrist to collect data. Based on previous research, cardiac activity provides features that could lead to accurate results of sleep monitoring. The interdependence of EEG and ECG signals have also been explored and showed some promising results. One pilot study on EEG and ECG activity in health and sleep apnea subjects reveals that the brain signal is more dependent in heart electrical activity. They suggest that the heart drives the brain activity [32] .

The portable devices for sleep monitoring discussed in the sections above can be classified into different types which are specified in Table 2.3.

TABLE 2.3: Classification of Portable Sleep Monitors[33]

Type I	Type II	Type III	Type IV
Standard PSG	Comprehensive Portable PSG	Modified Portable Sleep Apnea testing	Continuous single- or dual-bioparameter recording
Minimum of seven parameters including EEG, EOG, EMG, ECG, airflow, respiratory effort, oxygen saturation, and measures body position and leg movement (optional), requires constant supervision of a personnel	Similar to Level I, but no personnel	Minimum of four parameters including ventilation, heart rate or ECG, oxygen saturation. Body position and leg movements are optional. No personnel.	Minimum of one parameter. Body position and leg movement are not measured. No personnel.

2.2 Sleep Quality Enhancement Methods

Several methods of enhancing sleep quality are presented in this section. Sleep disorders are caused by numerous events such as recurring sleep deprivation and stress. There are various approaches to prevent and treat of sleep disorders.

2.2.1 Pharmacological Solution

Pharmacological approach in treating or preventing sleep disorders is widely used. These hypnotic drugs are known to induce sleep and increase SWS stage of sleep, especially for those who suffer from insomnia. However, risks in taking these drugs include dependence and residual daytime side effects.

2.2.2 Neurofeedback Training

Neurofeedback training (NFT) is a procedure used in manipulating brain activity or oscillations for different applications such as sleep enhancement. The reliability of NFT and the technologe have received some criticisms. As a response, Zoefel et al proposed three criteria in determining the reliability of NFT: trainability, independence, and interpretability [34].

Brain stimulation, by applying a small current through the brain, is a standard psychological procedure and was first introduced over 200 years ago [35]. Transcranial direct current stimulation (tDCS) and transcranial magnetic stimulation (TMS) are two non-invasive methods that are used in inducing current through different areas of the brain and has been proven to have significant applications in neuroscience. These methods can improve cognitive or memory performance and even treat some mental disorders. Moreover, the application of these methods in manipulating sleep quality has also been explored.

Different neurological parameters such as delta and alpha power spectrum are associated to various behavioural and cognitive functions. The dominant presence of alpha brain waves suggests that the brain is in the Alpha state or relaxed state[36]. In application, the alpha brain signal can be used to differentiate between wakefulness and drowsiness. The delta waves are seen in NREM stage 3 and 4 of sleep which also suggests that Slow Wave Sleep is the deep or restful sleep stage. Therefore, manipulation of the brain signals by extending the SWS stage could result in improved cognitive performance and restfulness of the subjects. As a result, many researchers have been interested in increasing the deep sleep stage which can be achieved by brain stimulation or brain training.

Another approach in non-invasive brain manipulation is the use of auditory and visual stimulants. These are realized by generating a series of light pulses and sound waves corresponding to a specific frequency. The subject's sensory receptors change the stimuli into electrical signal which is sent to different areas of the brain for processing. A study supports the claims that the brain wave bands are affected

by light and sound stimulation [37].There are devices such *Dreem, Rhythm, Mind Spa, and Mind Machine* that implement auditory and/or visual stimulation which claim to enhance sleep, reduce stress, improve short term memory, and more.

2.2.3 Micro-current Skin Stimulation

The application of sub-threshold current stimulation on the palm skin to improve sleep quality has been successfully demonstrated [8, 38]. In order to use this approach, a research to study electrical safety in designing a wearable device is performed. This section summarizes the different studies which identifies the safe amount of voltage that can be applied on the skin.

Stratum corneum is the outermost layer of epidermis that mainly consists of dead cells and is considered as the main contributor for the skin's high resistance. For broken and wet skin, the resistance can be expected to be lower as the 'salty' and wet layer underneath the skin is very conductive. The results of a study which compares the effects of short, high-voltage and long, medium voltage pulses on skin electrical and transport properties showed that the pulsing protocol with 20x(100 V – 100ms) and 20x(100V – 300 ms) had rare to no LRTs [39]. LTR or localized transport regions are created on the skin by electroporation. Another study investigated the tissue damage that can be induced by pulsed electrical stimulation as a function of pulse duration, electrode size and number of pulses. They used a fluorescent assay on chick chorioallontoic membrane (CAM)[40]. They concluded that the threshold current density j relates to pulse duration t as j α t-0.5 and is independent of electrode size for diameters greater than $300\mu m$. A set maximum voltage that is safe for the human body was not established as damage is only directly related to current. However, some studies show that with higher voltages, short pulse duration is preferable to avoid damage of the skin from heat. Also, for this project, the effect of voltage can be neglected as the palm generally has thicker layer of dead skin and the voltage stimulation is going to be applied in very short pulses.
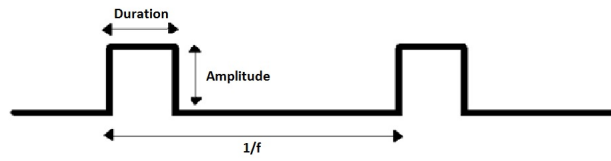
FIGURE 2.2: Pulse Parameters

2.2.3.1 Pain Sensation Threshold Associated with Electrocutaneous Stimulation

The introduction of stimulation current to the skin may lead to irritation and pain sensations. The pulse parameters for stimulation are pulsewidth, pulse magnitude, and repetition rate as seen in Fig. 2.2. The pulse parameters for stimulation are calculated on the study performed by Mason. [41]. The experimental results showed that up to $600V$ can be applied to the skin for stimulation as long as the current stays in the microamperes range. Moreover, the pain sensations felt was due to thermal effect from high local current densities on skin areas with high conductivity. The formula in 2.1 represents the maximum current that will result to a high electrical energy dissipated on the skin from a train of electrical pulses.

$$ I = \left(\frac{k_1 \theta_\tau A}{R t_p f} \right)^{\frac{1}{2}} \tag{2.1} $$

where:

I: is current in ampere

k_1: is constant 4.184 J/cal

θ_τ: is threshold thermal energy density 250 mcal/cm^2/s

A: is area of the electrode in cm^2

R: is electrode resistance in ohm

t_p: is pulse duration in seconds

f: is pulse frequency

2.3   Research Direction and Challenges

A standard sleep monitor device consists of sensors, signal filters, feature extraction algorithm, analysis, and output (whether it's a quantitative measure of quality of sleep, sleep stages or length of deep sleep). Though many methods have already been proposed and studied, the continuous research for optimization on several aspects of the wearable device is an ongoing process.

A home-based non-invasive sleep study that produces accurate and useful data is the main objective of this research. If some abnormalities are seen or a trend in sleep pattern is noticed, sleep data can be sent directly to a sleep specialist for further analyses and tests. One advantage of the technology used in portable or home sleep monitoring is the implementation of wireless communication. These promote comfort and could also result to cleaner signals, less susceptible to movement artifacts caused by moving wires. Lee et al. proposed a design of a Body Area Network (BAN) controller and IC sensor for sleep monitoring [42]. The most common wireless communication protocol that is being used by commercial products is low-power Bluetooth 4.0 (BLE); other options include Zigbee and WiFi Direct. The sleep management device also has a potential to be a part of Internet of Things (IoT) research in biomedical field.

Power consumption is important because it dictates the battery life of the device. The portable sleep monitoring devices have to operate using batteries to have power isolation to avoid potential electrical shock. Decreasing power consumption depends of various parameters. The complexity of the algorithm chosen must be simple to reduce the required amount of computation.

Chapter 3

Design Methodology

3.1   Project Overview

From the previous chapter, several methods of monitoring and actively enhancing sleep were discussed. As a result of those findings, a set of functional requirements and preliminary device prototype were designed. This chapter introduces the overall functionality and architecture of the device. The proposed block diagram of the device prototype is shown in Fig. 3.1. Several sensors are embedded in the device to collect physiological signals during sleep that will be classified to detect SWS. During SWS, a series of microcurrent pulses stimulate the subject's palm skin. All the data collected and activity throughout the night's sleep are recorded and saved either locally or to the cloud.
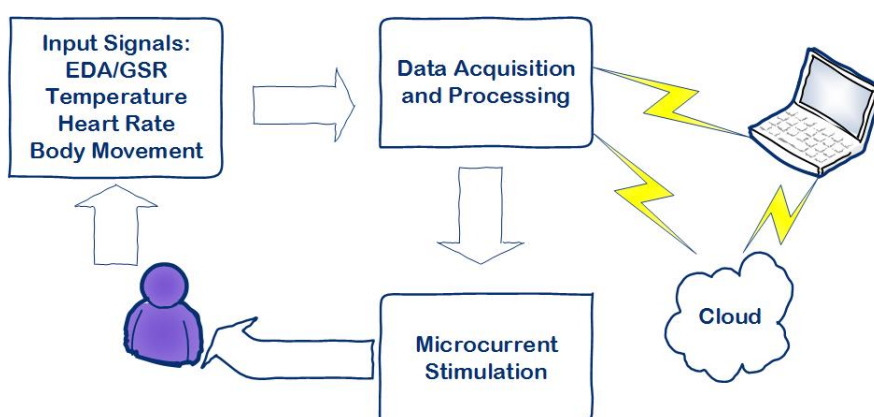
FIGURE 3.1: Project Overview

3.2   Device Specifications and Requirements

Several requirements are set based on the functionality of the device. Furthermore, sub-requirements pertaining to hardware, firmware and application are also established. The device prototype shall be capable of recording physiological sleep data such as EDA, body movement, ambient and skin temperature and heart rate. Low-power peripherals and microcontroller shall be chosen for better power consumption. The device must be able to remain functional for at least eight hours of operation. It must also provide sufficient storage for the data collected, and wireless connectivity. Lastly, a system to provide stimulation must be designed. A summary of the device specifications is shown in Table 3.1.

TABLE 3.1: Device Requirements

Parameter	Constraint
Processor	RISC architecture, low-power peripheral interface
Connectivity	microUSB for charging and data transfer & Wireless connectivity
Size	Maximum area of $36cm^2$
Power consumption and management	Support at least 8 hours of operation
Maximum stimulation current	$150\mu A$ at 100-300 ms duration at a frequency of $0.8 - 1.2$ Hz
Cost	Low cost
Storage	local, remote
Input signals	Body movement, EDA, skin and ambient temperature, heart rate

3.3   Rationale of Technical Solutions

The technical solutions to satisfy the requirements outlined in the previous sections are presented and discussed in this section. Through the series of design evaluation, a final prototype design will be established. These solutions are presented in Hardware Development and Software Development sections below.

3.4   Hardware Development

The wearable device requires a hardware design which includes the selection of sensors that will measure the sleep signals, storage, connectivity and processor. These hardware components are carefully analyzed to check if they meet the requirements of this project. Each subsection of this chapter discusses the options and what was chosen based on the features and ratings of the component.

3.4.1   Processing

The device shall have a processor unit which is responsible in controlling all peripherals and performing calculations for data analysis. The microcontroller needs to be high in performance, fast processing and low power functionality. As a result, a microcontroller with ARM architecture which runs in RISC (Reduced Instruction Set Computing) is preferable. Several microcontrollers have been considered based on the said hardware characteristics as shown in Table 3.2. Moreover, the ease of firmware development is also considered. The STM32L4 series microcontroller from ST Microelectronics was chosen since it meets the required functionality. The STM32L4 series is an ultra-low power, 32-bit, with ARM Cortex-M4 core microcontroller unit (MCU).

TABLE 3.2: Microcontroller Options

	STM32L4	STM32F4	MSP430F5	MK64FX512
Core	32-bit ARM Cortex M4	32-bit ARM Cortex M4	16-BIT RISC	32-bit ARM Cortex M4
Current Consumption	39uA/MHz	1mA/MHz	100uA/MHz	250uA/MHz
Max Clock speed	80MHz	168MHz	48MHz	120MHz
Flash Memory	1MHz	1MB	512kB	1MB
Manufacturer	ST Micro-electronics	ST Micro-electronics	Texas Instruments	NXP

A low-power ARM-based ST Micro STM32L476 will be used for data processing and peripheral controls of the device. The core of the microcontroller 32-bit ARM Cortex M4, which runs in RISC architecture for higher performance and lower power consumption. Several peripheral communication interfaces are also available in the device. An external oscillator of 8MHz shall be connected as external clock source, and the system source shall be set to maximum speed of 80MHz during device initialization. JTAG interface to the microcontroller will be used for programming and has to be made available in the hardware.

3.4.2 EDA measurement

One physiological signal that has a distinct characteristic used detecting SWS is Electrodermal Activity (EDA), as discussed in the previous chapter. EDA is a continuous analog signal that measures the electrical activity of the skin which is measured in volts. In the following sections, several configurations on measuring EDA are presented. The electrical model of the skin is shown in Figure 3.2
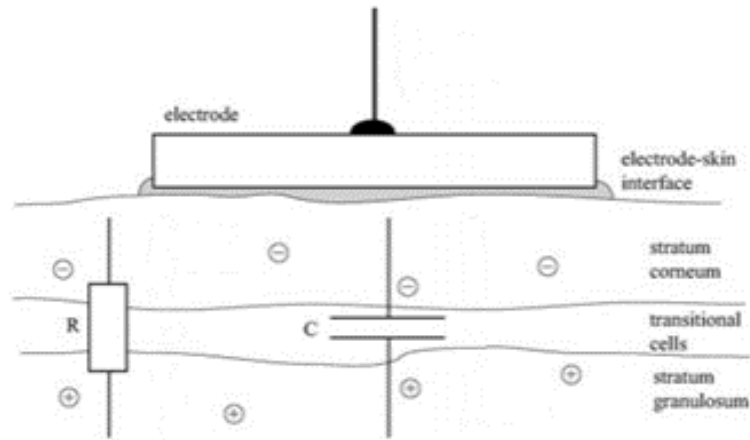
FIGURE 3.2: Skin Electrical Model

It can be seen that a simplified skin model consists of a resistor and capacitor network, in which the impedance is a function of frequency. However, the method of measurement that will be considered is by introducing a DC reference voltage or current. As a result, the frequency variable will be omitted and the skin conductance can be assumed as a purely resistive entity. Therefore, the following configurations are based on the assumption that the skin resistance measurement will be represented as a resistive parameter. Another parameter that is important to understand in the structure of the skin is the skin conductance and potential which has a range of $1 - 40\mu$Siemens and $10 - 20$mV respectively [24].

3.4.2.1 Constant-Voltage and Constant-Current Configuration

The two simple methods in measuring an unknown resistance is by utilizing Ohm's law, where the voltage is directly proportional to the current by a factor of resistance. If either voltage or current is controlled or used as reference, then the resistance can be calculated by the measured voltage or current.

In the constant voltage configuration, a precision reference DC voltage source is required. Voltage regulators are good examples of controllable constant voltage source. Some designs also include an operational amplifier to produce a feedback controlled reference voltage. The current flowing through the skin has to be kept

in minimal when an electrical potential is applied. To ensure that the current is kept to a minimal, a resistor with a relatively high resistance compared to the skin resistance can be connected in series. This creates a voltage divider to reduce the potential on the electrode in contact with the skin. An example measurement circuit with a reference voltage, a divider resistor and series of signal filters are shown in Figure 3.4. A wheatstone bridge, as shown in Figure 3.3, is another constant voltage circuit that measures unknown resistance. Three resistances $R1, R2, R3$ are known except Rx, which could be the unknown skin resistance. The $R2$ is an adjustable resistor which matches Rx if the voltage across nodes B and C is $0V$. This configuration is difficult to implement for this system as it requires an potentiometer to determine the value of Rx.
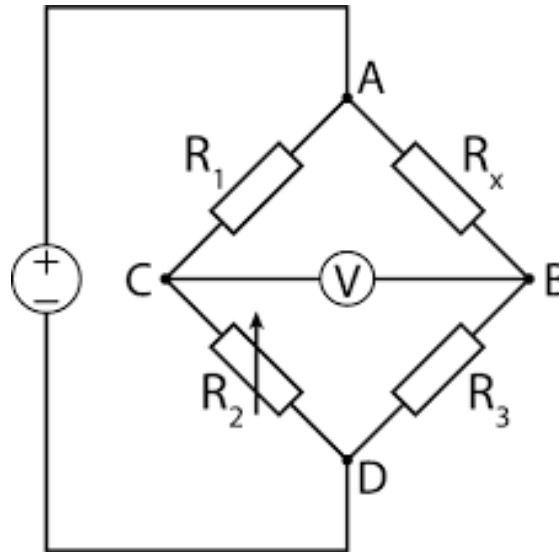
FIGURE 3.3: A Wheatstone Bridge

On the other hand, a constant current source can be used as the independent variable in measuring EDA. This method uses the same relationship as the constant voltage method. The disadvantage of using a current source is the measurement range when it is converted to voltage by the ADC. In order to investigate the feasibility of using a constant current for measurement, several current source chips and designs are explored. There are current source and sink design using an operational amplifier and complex integrated circuits with programmable output.

An example of such circuit is PSSI202ISAY constant current source from NEX-PERIA (previously NXP). The IC is programmable by an external resistor with an output range of $15\mu A$ to $50mA$ using equation 3.1. The design parameters that have to be considered are supply voltage and load resistance. If the supply voltage is set around $3V$, from the battery supply and the minimum current is $15\mu A$, the maximum skin resistance that can be measured before reaching saturation is 200 kΩ. This corresponds to a maximum measurement of 5μSiemens of skin conductivity. The minimum possible current value from this chip does meet the requirements of this project, but it is marginal as it saturates the measurement at high resistance value.

$$I_{out} = \left(\frac{0.617}{R_{ext}}\right) 15\mu A \tag{3.1}$$

The calculation discussed above can be modified to better meet the desired functionality. One option is to add a current divider by adding a resistor parallel to the load. In this case, the current will be distributed among the parallel resistors and the load, and it limits the saturation of the ADC when measuring high skin resistance.

The EDA circuit can be connected to the ADC following either single-ended or differential configuration. The number of bits of the ADC is also important. Table 3.3 summarizes the resolution of the ADC when the reference voltage is 3.3 volts.

TABLE 3.3: ADC bits and Measurement Resolution

ADC bits	Resolution (μV)
8	12890.63
10	3222.656
12	805.6641
16	50.354
24	0.1967

Since the range of the measurement is large and the changes in SCR peaks has to be captured, a high resolution 24-bit Sigma-Delta ADC is chosen to measure this signal. The AD7791 chip will be set to function in differential inputs and

will communicate with the microcontroller using SPI interface with bus speed of at least 5MHz. An analog-front-end (AFE) single order low pass filter in each differential input has to be included to remove high frequency noise and should also provide current path to ground that serves as protection circuit. Figure 3.4 illustrates the EDA measurement circuit, and the corresponding equation 3.2 in calculating skin resistance. The hardware shall provide external connections for electrode wiring. The electrode used is a 10mm diameter stainless steel.
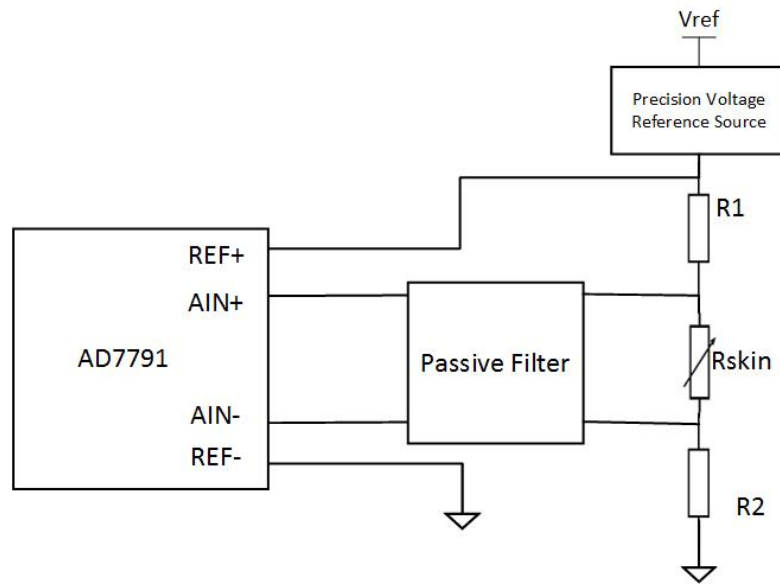
FIGURE 3.4: EDA Measurement Circuit

$$R_{skin} = \frac{R_1 + R_2}{\frac{V_{ref}}{V_{diff}} - 1}$$
(3.2)

3.4.3 Actigraphy

Another very popular non-invasive method in determining sleep quality tracking the subject's movement overnight. Actigraphy is a method that uses accelerometers to track movement which is mainly used in wrist-worn sleep monitoring devices. This adds accuracy in detecting which stage of sleep the subject is in. In choosing the accelerometer sensor, several parameters were considered. First, it is preferable to have at least three-axis measurement. There are numerous of options
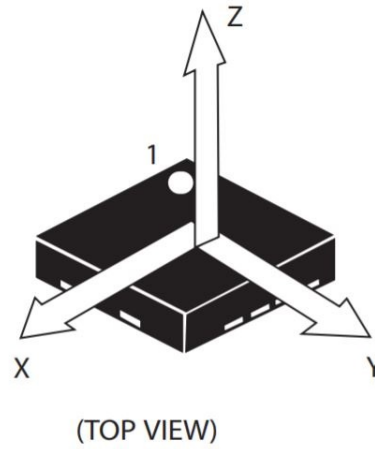
FIGURE 3.5: Direction of Detectable Accelerations

available for the accelerometer,but LIS2HH12 was chosen for this project because of it's low power performance, scalability, and small footprint. The directions of detectable accelerations for this component is in Figure 3.5.

The magnitude of the accelerometer represented as A in 3.3 will be used in determining the overall movement of the user. The accelerometer's range can be modified to $\pm 2g, \pm 4g, and \pm 8g$.

$$A = \sqrt{X^2 + Y^2 + Z^2} \tag{3.3}$$

One method in determining the movement and orientation of the subject is calculating the angle of the acceleration vector with respect to the X-Y plane. During sleep, where the regular movement is a subtle toss-and-turn motion and minimal rapid acceleration, the earth gravity acceleration will be the dominant reading of the sensor. If the skin is assumed to be X-Y plane, and the axis perpendicular to the skin is Z-axis, a reference for the angle measurement is established. The general angle (in degrees) calculation for this set up is in 3.4.

$$A = \frac{Z^2}{\sqrt{X^2 + Y^2}} * \frac{180}{\pi} \tag{3.4}$$

An accelerometer by itself may result to misdetection of sleep stage when the user stays still for a certain period of time. Therefore, this sensor data is integrated with other embedded sensors' data for better detection of deep sleep.

3.4.4 Heart Rate and Blood Oxygen Level Measurement

As discussed in the previous chapter, the heart activity provides several features that are useful in sleep monitoring. Electrocardiography is an accurate technique in measuring heart activity. The conventional setup in ECG measurement includes three electrodes around the heart: left side, right side and right-leg drive for biasing. The structure of electrode placement for accurate heart activity measurement is infeasible for this project. As a result, a less complex technique in measuring heart rate is chosen. The heart rate measurement system has to be embedded in the wearable device; thus, a miniature pulse oximetry sensor was chosen to measure heart rate.

Photoplethysmogram (PPG) is the process of collecting data optically using a pulse oximeter sensor. Light is shined through the skin and the change in light absorption is measured. A vital biological data for health monitoring is the heart rate and blood oxygen level (SPO2) of a person. MAX30100 by Maxim Integrated will be used to collect data. The sensor has a built-in temperature sensor and interfaces to the microcontroller via I2C bus. The block diagram of the internal circuitry is shown in Figure 3.6.
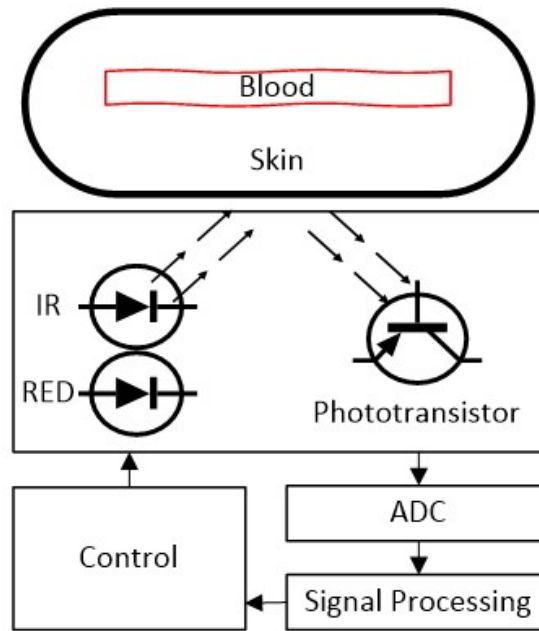
FIGURE 3.6: PPG Block Diagram

The sensor consists of two RED and Infrared LED sources. The wavelength of these sources determines the quality of data being collected. The wavelength of IR LED is 880 nm while RED LED is 670 nm. The light absorption spectra of hemoglobin as seen in Figure 3.7 which shows the molar extinction coefficient as a function of light wavelength. The figure suggests which of the two LEDs is more accurate in measuring either oxygenated or non-oxygenated blood. The internal ADC resolution is set to 16 bits but can be reconfigured in the register by changing the LED pulse width setting. The sensor performance is tested by varying several parameters such as pulse width, sampling rate, LED current and configurations.
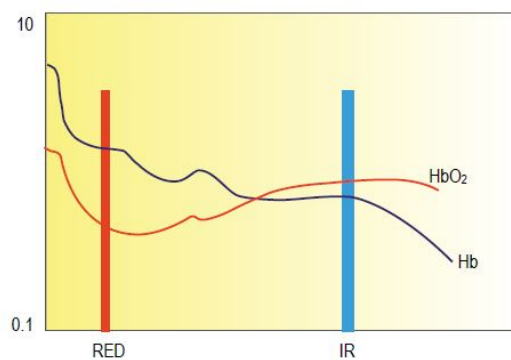
FIGURE 3.7: PPG Block Diagram

3.4.5 Electro-stimulation

Two systems are developed to apply stimulation to the palm: high voltage and direct current. Both provide flexibility in stimulation as frequency and amplitude can be controlled in the microcontroller.

3.4.5.1 DRV2700 Voltage Driver

One option in providing electrocutaneous stimulation is by supplying voltage potential stimulus. The DRV2700 chip was chosen to provide the pulsed excitation because it offers control options in several parameters such as gain, period and output voltage levels.

Figure 3.8 is the schematic model for the voltage stimulation system. A resistor network sets the boost output voltage by modifying the connections of the resistors. The boost voltage is set to $105V$ but can be reduced by removing or adding resistors in the resistor network. Moreover, the boost current can be limited by

$$R_{ext} = \left(K \frac{V_{REF}}{I_{LIM}} - R_{INT} \right) \tag{3.5}$$
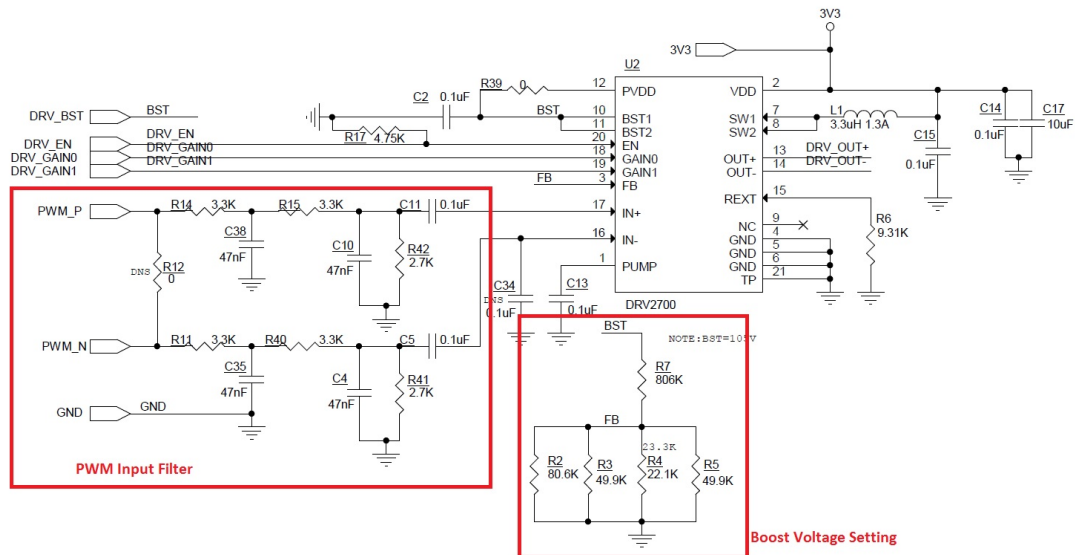
FIGURE 3.8: Piezo Driver Schematic

Similar to the other peripherals, the microcontroller controls the chip using GPIOs and PWM. The gain options available are 28.8 dB, 34.8 dB, 38.4 dB and 40.7 dB which is programmed by GPIO pins DRV_GAIN0 and DRV_GAIN1. The input signal is PWM generated by the microcontroller and will be amplified according to the set gain. The boost voltage becomes the supply of the amplifier which makes the voltage rail setting. Since the output could be differential, the maximum peak-to-peak voltage output could be up to 200V.

Table 3.4 shows the default settings of the DRV2700 chip.

TABLE 3.4: Default Settings

Parameter	Value	Control Pins
Boost Voltage	105 V	Resistor Network (HW)
Gain	28.8 dB	PA9, PA10 (SW)
PWM	Frequency: 0.5-1.2Hz, Duty cycle: 20%	PA6, PA7

3.4.5.2 LT3092 Constant Direct Current Source

Direct current stimulation is being used in medicine for different applications. A direct current source is integrated in this device to as an option in palm stimulation. A programmable current source LT3092 from Linear Technology was chosen. The internal circuitry and design is in Figure 3.9 and the output current is designed by setting the values of the series and output resistors as in 3.6.
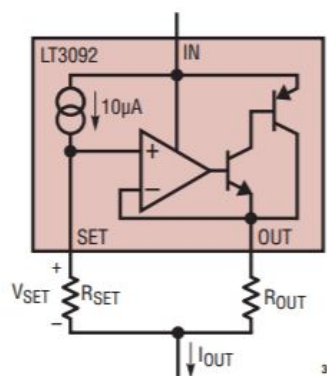
FIGURE 3.9: LT3092 Internal Circuit

$$I_O = \frac{V_s}{R_o} = \frac{10\mu A * R_s}{R_o} \tag{3.6}$$
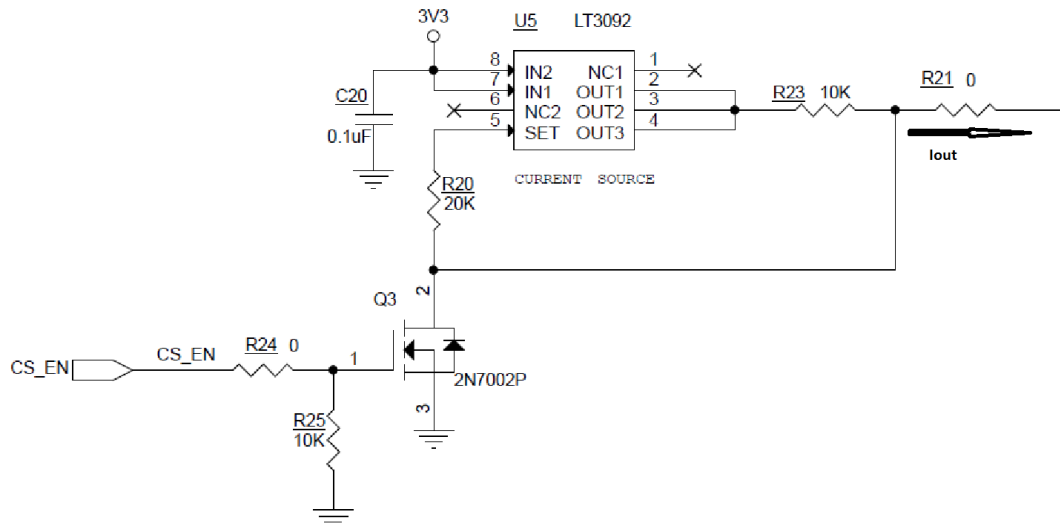
FIGURE 3.10: Current Supply Schematic

The design schematic for the constant current source is in Figure 3.10. The resistor values used are Rs=10kOhm and Ro=20kOhm respectively, which result to $20\mu A$ current output. This is below the current threshold for pain in electrostimulation. The microcontroller GPIO controls the output of the current source through cs_en pin which is connected to the gate of the MOSFET. A series of timed pulses can be generated in the code to set the frequency of the pulses.

3.4.6 Power Supply

Linear Technology LTC4099 I2C Controlled USB Power Manager/Charger with Overvoltage Protection will be embedded in the device. The power supply of the system is connected to external supply using a microUSB connector. The IC will provide the 3.3V system rail for all the subsystems downstream and also charge the built-in Li-Ion or Li-Polymer Rechargeable battery. In addition, LTC4099 interfaces with the microcontroller via I2C interface to modify chip register settings

and read power supply status. The maximum charge current is 1.5 A, and a thermal limiting capability can be utilized. The diagram for the power supply is shown in Figure 3.11. Appedix C shows a template to calculate the power consumption of the device.
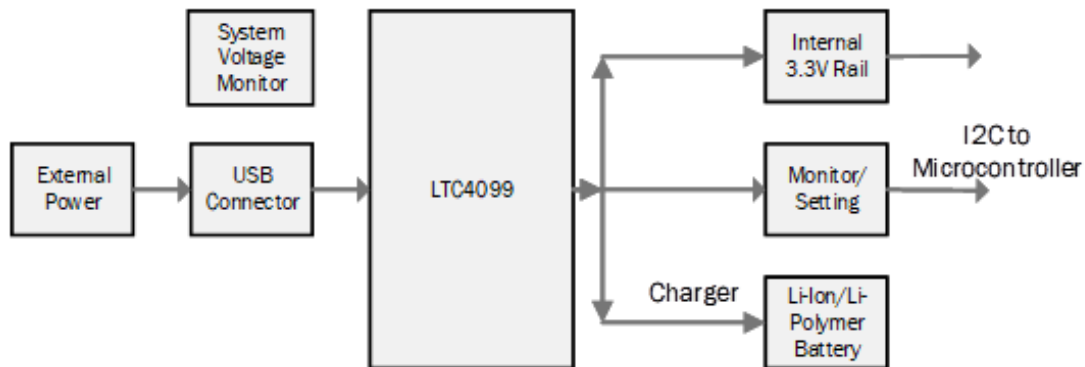
FIGURE 3.11: Power Supply Block Diagram

3.4.7 Wireless and Local Storage

The wearable device requires location for data storage whether locally or in the cloud. Thus, an Secure Digital (SD) card slot and WiFi module are added to the design to provide these functionalities. A microSD card can store the data locally overnight. A third party software called FatFS controls the filesystem creation and access to the memory. The micro-SD card module communicates with the microcontroller via SPI interface. Each write/read transfer is done in 512byte block. The subsystem can support SD Cards up to 64GB memory.

On the other hand, ESP-01 WiFi module which embeds an ESP8266 chip was chosen to provide wireless communication. Compared to Bluetooth Low Energy (BLE) which has less power consumption, a WiFi module was chosen to remove the dependency on a third device. The compatibility between platforms when developing an application for bluetooth connection introduces complexity in the project. The WiFi module provides direct connection to the web which makes the device a part of Internet of Things (IoT). An AT-command firmware is flashed in

the chip for built-in commands corresponding to different layers of the Transmission Control Protocol/ Internet Protocol (TCP/IP). As seen in Figure 3.12, the corresponding protocol in the application layer, transport layer, network layer and data link layer are HTTP, TCP, IP and Wi-Fi respectively. The ESP8266 module can be set as a server or a client. In this application, the module acts as a client which connects to a local server to dump binary data. One option in pushing data to the web is using Hyper Text Transfer Protocol (HTTP) commands, which are POST and/or GET request. The steps in transferring data is shown below. Wireshark software, a Wi-Fi packet sniffer, was used to analyze the packet transmission and reception from the device to the local server and vice versa. Local hosting was implemented using the program MAMP. Algorithm 1 shows the steps in connecting to a server using the WiFi module.
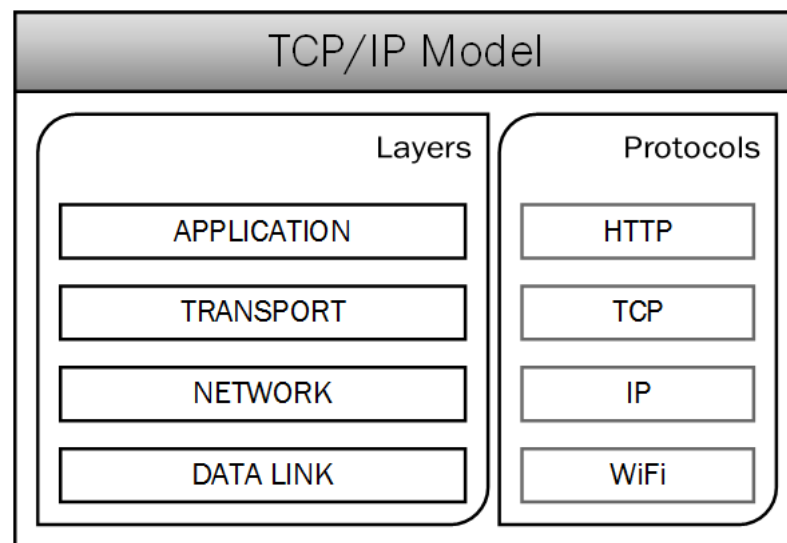
FIGURE 3.12: TCP/IP Stack on ESP8266 Module

Algorithm 1 Steps in Wireless Data Transfer

$InitializeWiFimodule$

procedure CONNECTING TO INTERNET

    if Connected to Access Point **then**

        $Connecttoserver$

        $Readresponse$

        if Successful connection **then**

            $Sendmessagepacket$

            $Readresponse$

        end if

    end if

end procedure
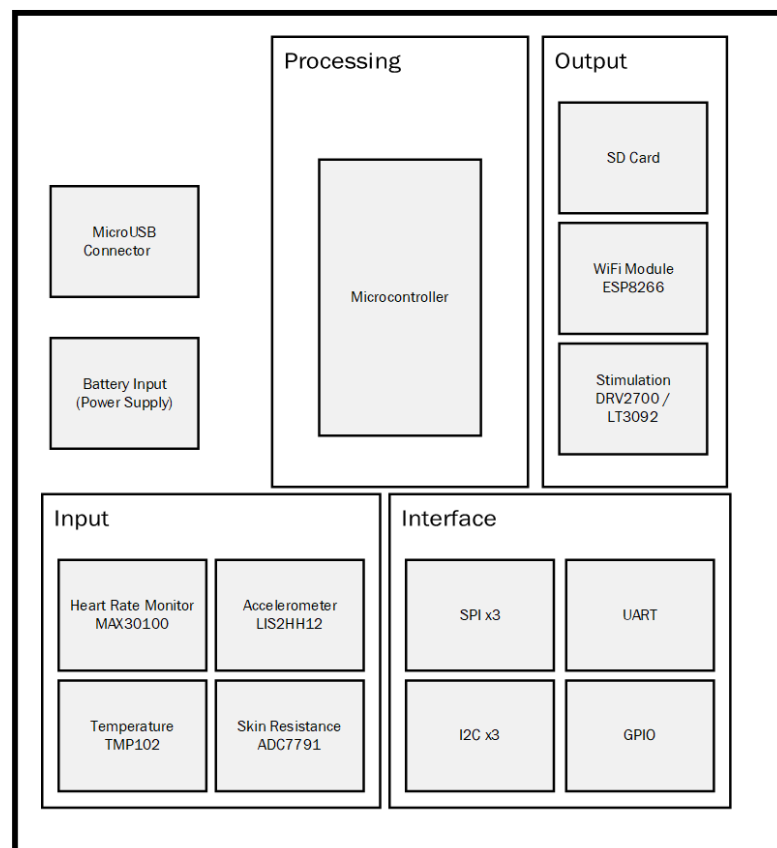
FIGURE 3.13: Hardware Block Diagram

Various hardware solutions are introduced in this section. The components are evaluated in terms of overall functionality to meet the requirements for this project. The chosen sensors, microcontroller, and storage circuits are put together to build the device prototype. The hardware components of the prototype device are shown in block diagram in Figure 3.13. The sensors will collect physiological signal such as heart rate, EDA, skin and ambient temperature and body movement during sleep. A power supply with USB connectivity is also embedded in the device.

3.5   Software Development

The software development of the prototype device includes the drivers and application code. This chapter introduces the code written for this device including the third-party softwares that are utilized for faster development. The software architecture follows the ARM design as the microcontroller chosen has an ARM-Cortex core. These software layers are shown in Figure 3.14 which summarizes the various parts of the firmware design of the project. The lowest level consists of the hardware peripheral drivers which are written for interfacing and data collection. The driver includes but not limited to initialization, access to register settings, and interfacing functions to the microcontroller. Low level drivers are written for the following peripherals.

Peripheral Drivers

- MAX30100 - Heart Rate Monitor

- TMP102 - Temperature Sensor

- MCP79410 - Real Time Clock

- AD7791 - Analog-to-Digital Converter

- LIS2HH12 - Accelerometer

- ESP8266 - WiFi Module

Next layer is the Hardware Abstraction Layer(HAL) code from the manufacturer ST Microelectronics. The package has the methods or functions to access or control the features and functionality of the microcontroller. The GPIO, communication interfaces, USB, power mode are few of the main functions that can be accessed. A wrapper to the HAL interfaces is written to match the sensor drivers which are written in C++. Next layer includes the third party software FatFs and FreeRTOS which include complex algorithm in the functionality of filesystem and operating system respectively. Some utilities and CMSIS code which essential piece in developing the software are utilized throughout the layers. This layer has the configuration and functions for memory allocation, system clocking, and threads. Lastly, the very top of the software architecture is the application code. All the other layers are integrated in the application layer to program the overall functionality of the device.
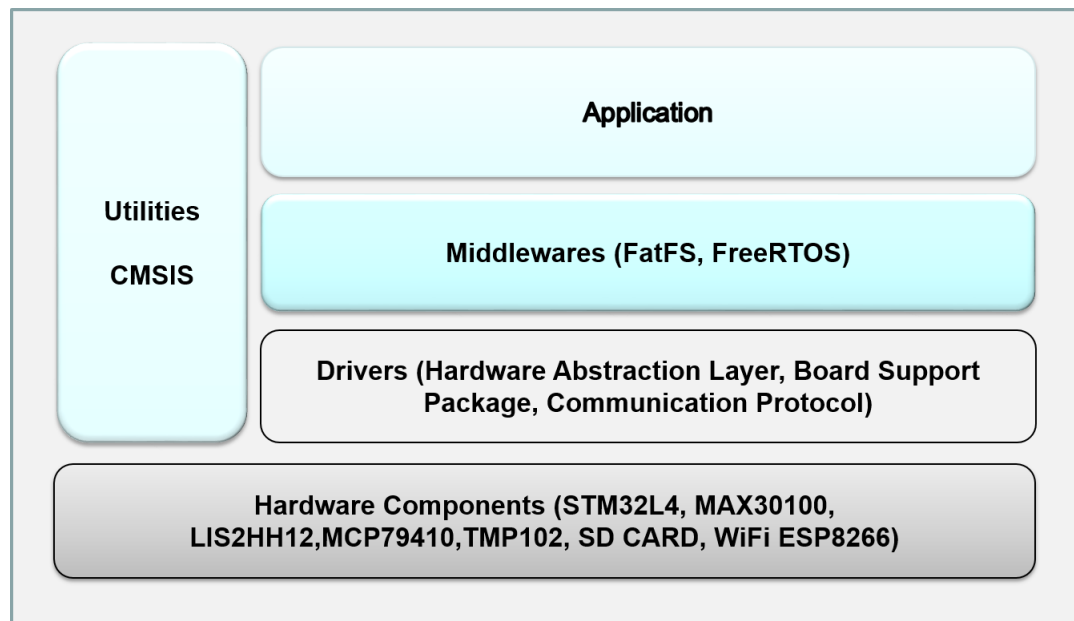
FIGURE 3.14: Software Architecture

3.5.1 FreeRTOS

An operating system (OS) is a software application which makes it seem like processes are running simultaneously. Technically, the processor core can only run a process one at a time; however, the complex algorithm for task scheduling makes

it efficient to run multiple processes for a given time span. The process could also be called a task or thread. A thread can be event driven or scheduled/timed. FreeRTOS is an open-source software implementation of a Real-Time Operating System (RTOS) developed mainly for microcontroller programming. FreeRTOS has an efficient scheduling, task creation, memory allocation and low program footprint which makes it suitable for embedded applications. An Application Program Interface (API) wrapper is written over the FreeRTOS software for this device.

3.5.2 FatFS

FatFS is a third party generic File Allocation Table (FAT) filesystem for efficient interfacing of the device to the SD card module to save collected data locally. FatFS provide application interfacing functions that allow the embedded device to perform filesystem actions such as creating, reading and writing files.

3.5.3 Data Handling

A global data container is required in an RTOS system since variables inside a task is not accessible to other tasks. The FreeRTOS package have an implementation called Queue where tasks can write and read data. A First-In-First-Out buffer array that contains struct of sensor data samples for one second was implemented. The read_sensor task writes a FIFO entry every second. On the other hand, the write_sd_task takes data from the buffer to write in the SD card. Similarly, all the other task can access the buffer as long as a task is not using it. The locking mechanism is implemented using mutexes. This makes sure that only one task has access to the buffer at any given time. The data acquisition sampling rates are set as in Table 3.5

TABLE 3.5: Sensor Sampling Rate

Signal	Data Rate
EDA	10 Hz
Heart Rate	50 Hz
Temperature	1 every 30 seconds = 1/30 Hz
Accelerometer	1 Hz

```cpp
struct FifoItem_t
{
sys::date_time_struct dt;
uint16_t hr[50];
uint32_t eda[10];
float accel[10];
float temp;
};


const size_t FIFO_SIZE =30;
FifoItem_t fifoArray[FIFO_SIZE];
```

LISTING 3.1: FIFO Buffer Structure

3.5.4 Communication

Each peripheral is connected to the microcontroller through the interfaces described in this section.

3.5.4.1 I2C

Inter-Inter Communication (I2C) is one of the peripheral interfaces that is utilized in this system. Each peripheral has a unique address, and the speed of the bus is be set to 400000Hz. Table 3.6 shows the peripheral sensors that share a bus.

TABLE 3.6: Components on the I2C bus

Peripheral	Bus
MAX30100, TMP102	I2C1
LIS2HH12, MCP79410	I2C2
TMP102, LT4099	I2C3

3.5.4.2   SPI

Serial Peripheral Interface (SPI) will be used to communicate with the peripherals in Table below. The speed of the bus shall be set to at least 5MHz communication with the sensors. Since block transfers are required for both SD card and display module, the software drivers shall be implemented using Direct Memory Access (DMA).

TABLE 3.7: Components on the SPI bus

Peripheral	Bus
AD7791	SPI1
SSD1306	SPI2
SD Module	SPI3

3.5.4.3   UART

The WiFi module ESP8266 has to be connected to UART TX and RX of the microcontroller. The baud rate is set 9600 bps.

3.6   Development Tools

Several tools used in developing the device's hardware and software are presented in this section. These tools are compatible with a Windows 10, 64-bit machine.

3.6.1 Orcad Capture and Allegro

Orcad Capture is a powerful design environment used for schematic design of electrical circuits. The program comes with wide library of symbol and footprints for common electrical components. However, symbols and footprints for a large portion of components needed for the design of the prototype were drawn for this project. A printed circuit board was developed for this project. The schematic and layout for the device prototype are designed using Orcad Capture and Allegro respectively. The size of the board was estimated using the footprint of the components with an additional allowance for spaces around. The package size of components were chosen to keep the board area relatively small.

3.6.2 Crossworks for ARM

The software development requires a complete C/C++ and assembly language system for microcontrollers, and the Crossworks for ARM is chosen for this project. Crossworks is a full Integrated Development Environment (IDE) for writing, building, downloading and debugging over SWD or JTAG. It is a GNU GCC toolchain which compiles C and C++ languages to be downloaded to the target. The toolchain provides libraries and packages specific in developing software for ARM-core microcontrollers. It also allows the ability to on-device debugging of the application code.

3.6.3 STLink V2

An in-circuit debugger and programmer device is required for communication between the STM32L4 target and the computer via a USB connector. The device incorporates features for JTAG and serial wire debugging (SWD) for debugging and programming the target.

Chapter 4

Results and Discussion

The multi-sensor device prototype measures physiological signals during sleep. The sensors are tested to investigate the data and to extract features that are significant for the study. The sensor results are presented and discussed in this chapter.

4.1 Experimental Results

4.1.1 Heart Rate

The correlation of heart rate and stage of sleep will be studied using this device; therefore, a heart rate monitor using pulse oximetry is integrated. The raw signal of PPG as shown in Figure 4.1 requires data processing to remove noise from power lines and baseline drift or DC component of the signal to properly detect the oscillation peaks. The selected data collection rate is 50Hz. To evaluate the data collected, a post processing in MATLAB is performed to analyze the behaviour of the PPG signal. The analysis also suggests the types of mathematical calculations that may be implemented in real time processing during sleep. Keep in mind that the objective of this project is perform the analysis in cloud to reduce the power consumption burden from the device.

In the post processing, a bandpass filter is implemented to filter out noise from the signal. The average resting heart rate for a human being is in the range of 60 to 100 beats per minute. Using this data, the filter is designed to have a cutoff frequency of 0.25 and 4 Hz, and order of 20. The algorithm for filtering the raw data and calculating heart rate is outlined in Algorithm 2. For pre-processing, the raw data goes through a bandpass filter and saved in a buffer with a window size of 500 for 10 seconds worth of data. In this window, the number of peaks are counted by finding the local maximum within the window. The validity of the peak is verified by checking the distance between two peaks which needs to be more than 0.2 seconds. If the period between two peaks is 0.2 seconds, the heart rate equates to 300 beats per second which is an invalid heart rate calculation. The heart rate calculated from a 10 second worth of data is extrapolated by adding the number of peaks of six consecutive windows.

An example of the processed data for one of sleep data from one subject is presented in Figure 4.2. The plot on top is the extrapolation by multiplying the number of peaks within the 10 second window by 6 to get beats per minute while the plot at the bottom is the moving average of the peaks over 6 consecutive windows. It is important to note that noise from artefacts caused by movement are not removed, and it contributes to the calculation of the heart rate. These artefacts introduce a significant error to the calculation that needs to be corrected for a more accurate result. However, based on preliminary data collected, the significance of heart rate data in the detection of SWS is yet to be established. For that matter, this platform will be utilized to collect sleep data for the study.

Algorithm 2 Calculating Heart Rate

1: **procedure** BEATSPERMINUTE(hr_raw)
2:   $hr\_filt \leftarrow hr\_raw$ $\triangleright$ Pre-processing
3:   **if** $buffer\_window != desired\_window\_size$ **then**
4:     append hr_filt to $buffer\_window$
5:   **else if** length($buffer\_window$) == $desired\_window\_size$ **then**
6:     find local maximums
7:     $hr\_cnt \leftarrow count\_of\_local\_maximums$
8:   **end if**
9:   $bpm+ = hr\_cnt[i]$ $\triangleright$ Sum of 6 consecutive hr_cnts
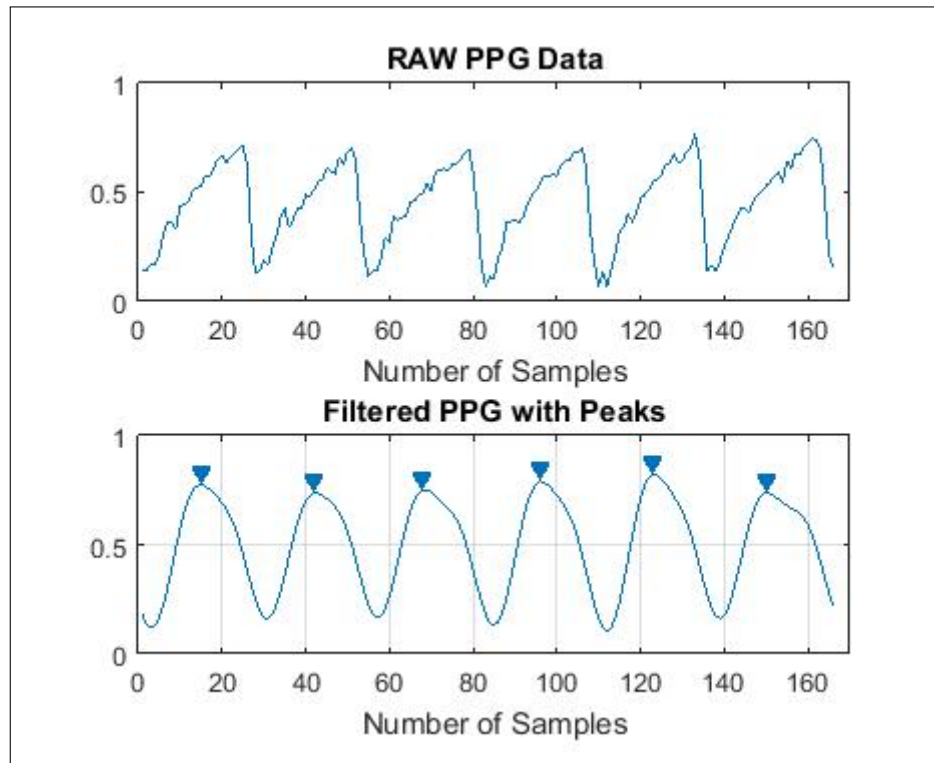10: **end procedure**
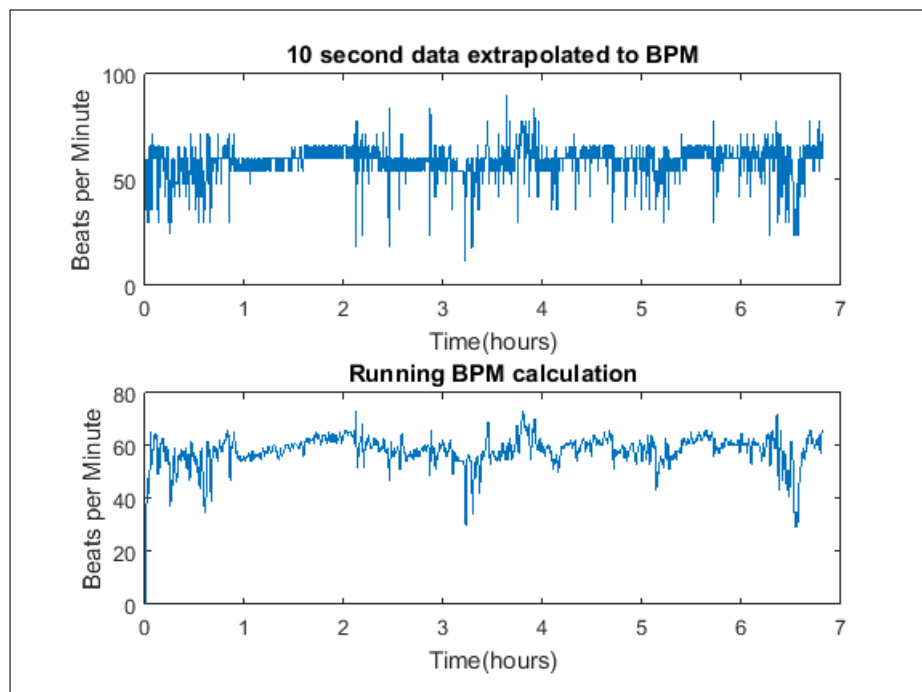

FIGURE 4.1: Raw and Filtered PPG Signal

FIGURE 4.2: Calculated Heart Rate during sleep

4.1.2   Actigraphy

This section presents the significance of accelerometer data during sleep. As mentioned in Chapter 1 of this document, body movement is correlated to sleep stages. Though not as accurate as an EMG or PSG, wearable devices in the market claim that actigraphy data is sufficient in identifying sleep stages. To investigate how accelerometer data would be analyzed and presented, several data analysis techniques were studied. Figure 4.3 presents the analyses performed to the raw data to extract useful information. The accelerometer data are converted in terms of g, earth's gravity $g \approx 9.81 m/s$. A sensor at rest will measure $1g$ towards the direction perpendicular to the ground.

The experiment shown in 4.3 can be divided into five different parts. The gravity acceleration of $1g$ is the baseline for the experiment. The method is turning the device to get $1g$ measurement corresponding to the direction it is turned to. Refer to Figure 3.5 for the detectable axes of the chip. First, leave the device on top of a flat surface so that the component is facing upwards. Next, turn it to the side to get the reading on the Y-axis, and then towards the X-axis direction. Afterwards, move the device randomly and slowly. Raw values from each axis are shown at the very top subplot of the figure. These raw data are then transformed to get the magnitude and angle with the Z-axis of the accelerometer. Lastly, the first derivative of the angle and magnitude were plotted to show the rate of change over the accelerometer data. The graph can be interpreted so that the flat line means no movement, and other readings show the intensity of the acceleration and change in angle.

From this simple experiment, it can be seen that the magnitude does not provide a strong representation of the movements. On the other hand, the angle is more informative of the movements. It can also provide information about the body position of the subject, since the component's Z-axis is perpendicular to the skin. Crossing the 0 can also indication a toss-and-turn movement. Moreover, a threshold value in terms of degrees with a range of $[-90°, 90°]$ is a better option.
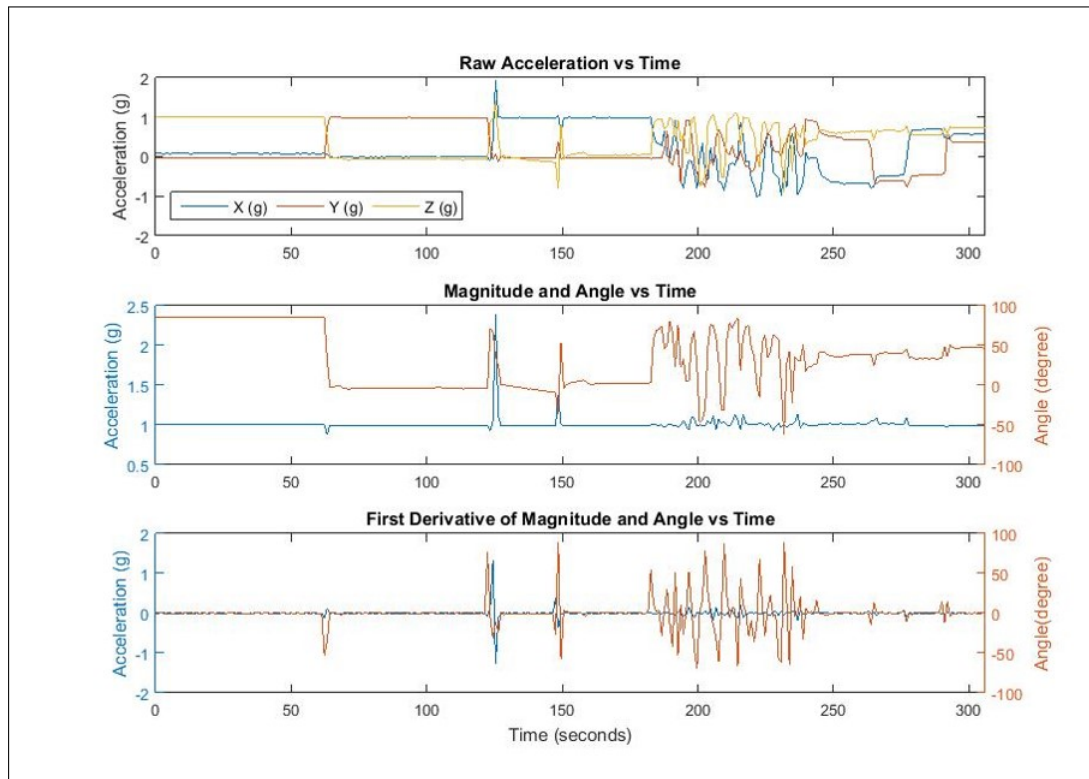
FIGURE 4.3: Raw and Filtered Accelerometer Signal

The focus of the study is to compare which feature provides a more distinct representation of body movement during sleep. According to the information from previous sections, there should not be any movement when the subject is in deep sleep. Therefore, every accelerometer reading that corresponds to a movement suggests that the subject is either in wakefulness or other stage of sleep.

4.1.3 Skin and Ambient Temperature

One of the objectives of developing this prototype is to study the feasibility of measuring the skin/extremity body temperature and ambient temperature, and if this information will be useful for identifying sleep stages. The results of few nights of data are presented in this section. One example is shown in Figure 4.4.
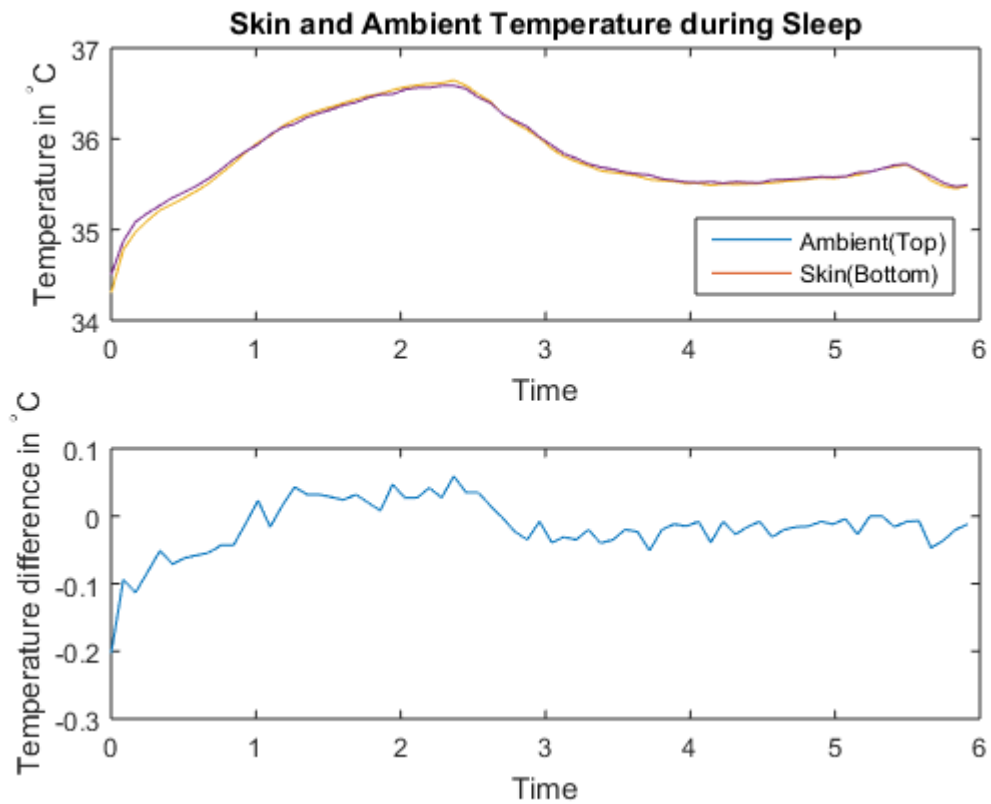
FIGURE 4.4: One night data of skin and ambient temperature during sleep

TABLE 4.1: Difference in Skin and Ambient Temperature during Sleep Test

Sample	Max Diff (°C)	Mean Diff (°C)	Max Diff (%)	Mean Diff (%)
1	0.2030	0.0319	0.5883	0.0890
2	0.0660	0.0329	0.1886	0.0935
3	0.2500	0.0313	0.7503	0.0891
4	0.1370	0.0182	0.4030	0.0515
5	0.9370	0.0438	3.2614	0.1293
6	0.2610	0.0330	0.7747	0.0948

The separation between the two temperature sensors is the thickness of the PCB. One has direct contact with the skin, while the other is exposed to the ambient environment. The results suggest that there is no significant difference ($< 1\%$) between the two sensors. As expected, there is low probability that accurate measurement of body temperature can be obtained from extremities. However,

ambient temperature may be a useful piece of information to indicate the sleeping environment of the subject. These results suggest that one temperature sensor is enough for the next revision of the prototype device.

4.1.4 EDA Measurements

In the previous section, various methods of measuring EDA were introduced. The 24-bit analog to digital converter, AD7791, was chosen to measure the electrical activity of the palm skin. The ADC measurement ranges from 0 to 3.3 V. The noise associated with quantization of the ADC is frequency dependent as stated in the datasheet. To minimize the introduction of noise, the update rate was chosen to be the slowest possible setting of 9.5 Hz. EDA activity is generally slow during sleep which makes the update rate sufficient for this application. The effective resolution for this setting is 22 bits.

The simulation for the skin measurement system using ideal values are in Figure 4.5. Notice that the plot is not linear because of the equation representing the measurement circuit is not linear. The circuit is simulated using LTSpice to predict the voltage and current reading of the chosen design. As seen in the figure, the voltage measurement of the first $300k\Omega$ of skin resistance ranges from 0.3 to 2.4 volts; and up to $1.2M\Omega$ at 3 volts. This corresponds with the range specified for skin conductance which is in the range of $1 - 40\mu$Siemens as presented in chapter 3.
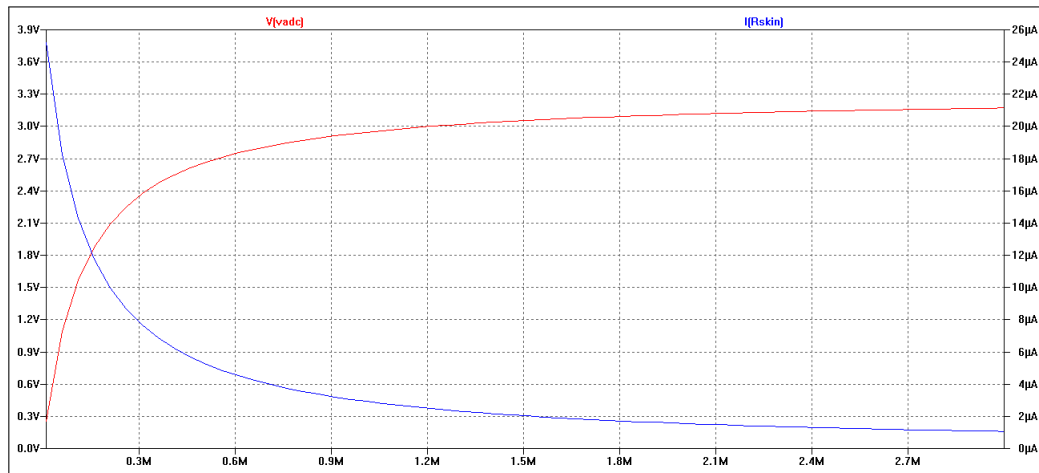
FIGURE 4.5: Differential Voltage and Current with varying Skin Resistance

Figure 4.6 shows an example of two EDA peaks measure from the palm using a sampling frequency of 10 Hz. For the purposes of this study and application, the accuracy of the sensor in terms of measuring the real value of the resistance is not the main focus. Rather, the ability of the sensor to catch the change in skin resistance during low frequency oscillations is more important. The data collected needs to be analyzed and filtered to remove the DC component or the baseline when measuring skin resistance.
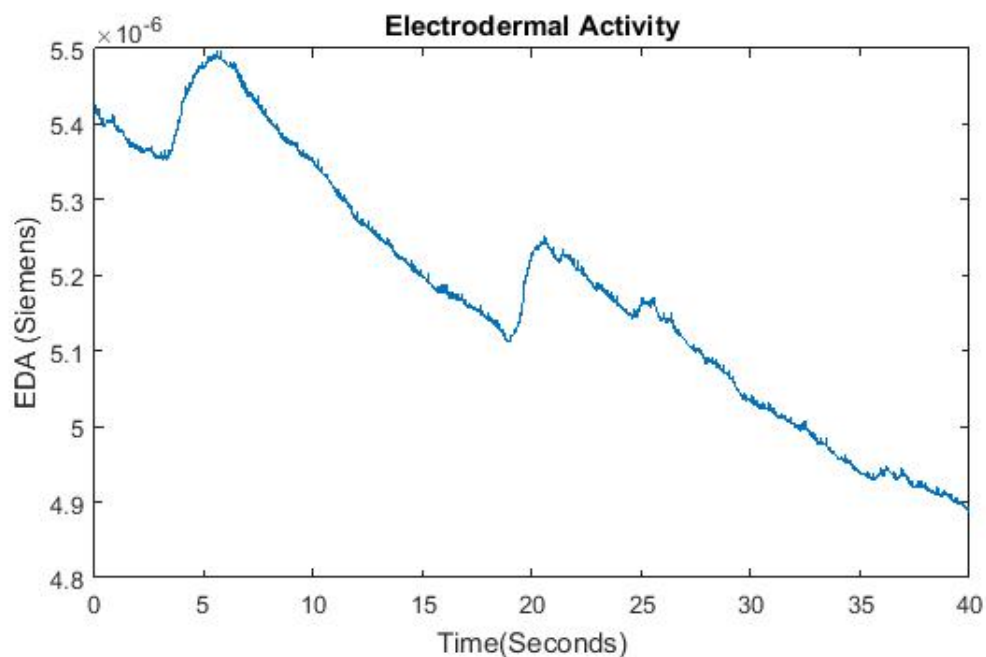
FIGURE 4.6: Raw EDA Signal

The EDA measurement circuit was evaluated by connecting the electrodes to the palm when the subject is awake. Figure 4.7 shows the data collected the skin resistance. The baseline is evident by the slope of the measurement. Also, no controlled stimulant was introduced to the subject so the validity of SCRs are not part of the study.
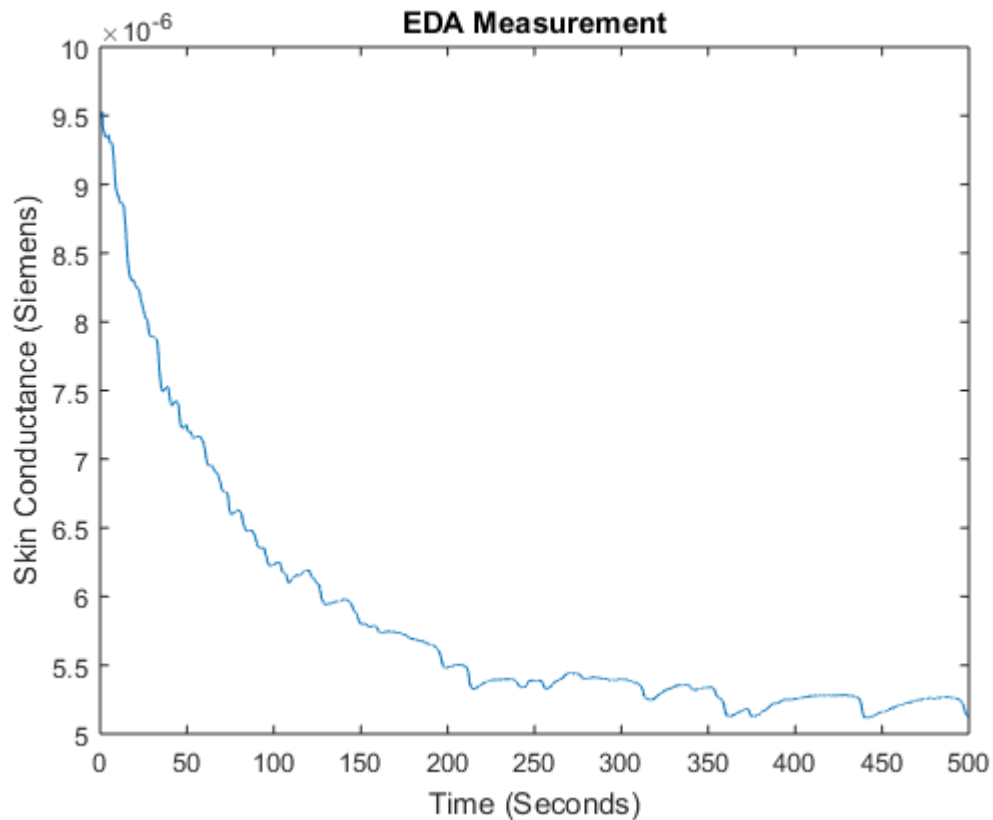
FIGURE 4.7: Raw EDA Signal

The derivative of the collected signal is calculated and plotted in Figure 4.9. The slope of the signal can be used as a threshold to mark a valid EDA peak. According to the EDA guide, the threshold for EDA peak is $0.04, 0.03$, and $0.01 \mu S$ are more common [24]. If five EDA peaks per minute for ten consecutive minutes are found, then the subject is considered to be in SWS. At this time, the low intensity stimulation will be applied to the palm skin.
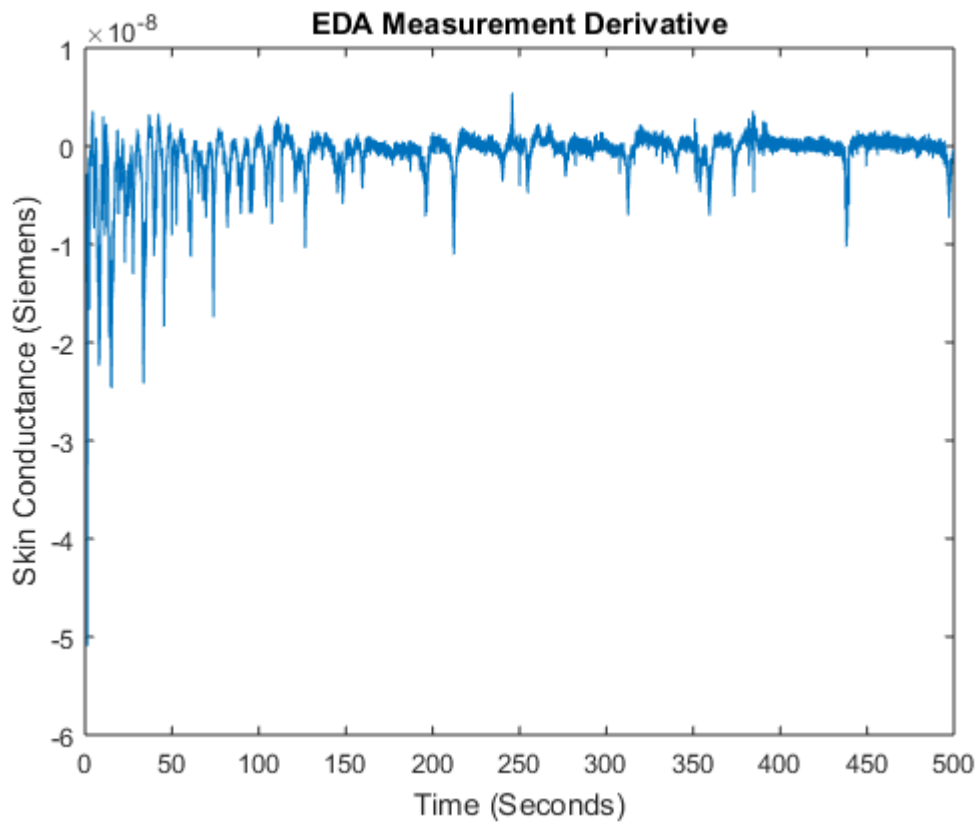
FIGURE 4.8: Derivative of EDA Signal

4.2 Electro-stimulation

The platform applies sub-threshold stimulation of the palm skin with low-intensity electrical pulses. Unlike CES, the electrical current is applied to the palm skin instead of directly to the brain. Using the equation in 2.1, electrode of 10mm diameter, electrode impedance of 5kΩ, pulse duration of 300 ms with frequency of 1.2Hz , the maximum current that will introduce thermal injury is 135mA. This value is significantly larger than the target 150μA stimulation intensity. Therefore, risk for thermal skin injury is minimal. As presented in the previous chapter, there are two implementation methods were presented: voltage or current source.

First, the current source discussed in previous chapter was investigated by simulation on LTSPice. The voltage rails at 3.3 V when the skin resistance is $\sim200k\Omega$

and current of $\sim 27\mu A$. With this set-up, the current is suppressed at higher resistance without a voltage boost. A voltage boost can be designed as an addition to the current source, or as an independent voltage source.
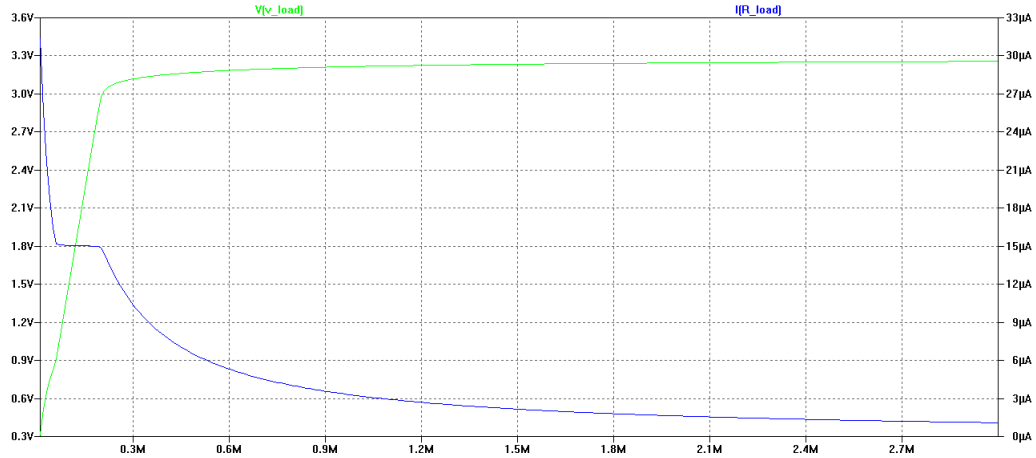
FIGURE 4.9: LT3092 Simulation

The other option is using DRV2700 piezo-driver which provides oscillating voltage with controllable gain and duty cycle. These parameters were investigated by connecting a constant resistance to the output of the driver. An example of the output voltage from the driver is shown in Figure 4.10. In this particular figure, the duty cycle is set to 50% with a frequency of 250Hz. The train of pulses have a period of 1 second. The output voltage and load is set to 38.4V and 899000 ohms respectively. As a result, the Math channel shows the current output.
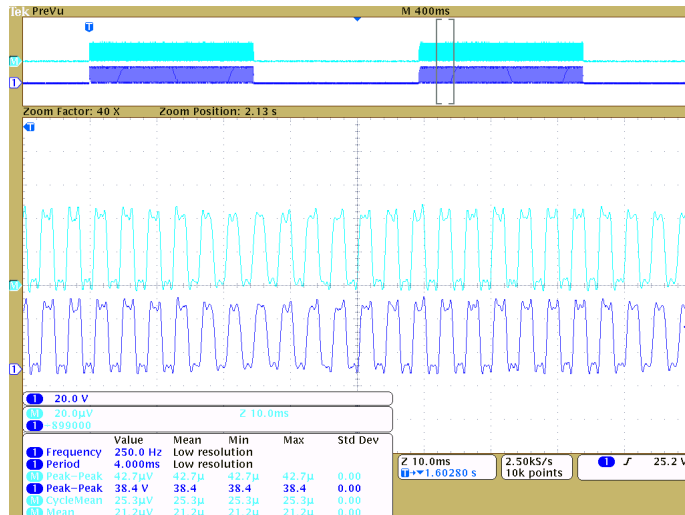
FIGURE 4.10: Example of stimulating signal
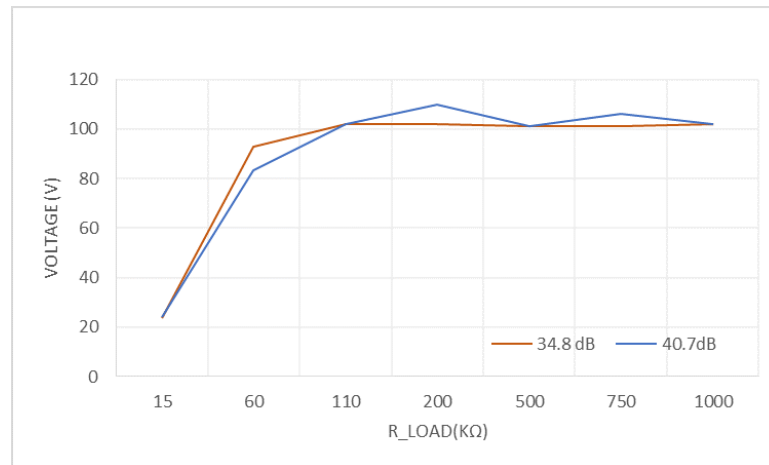
FIGURE 4.11: Peak voltage vs R_load
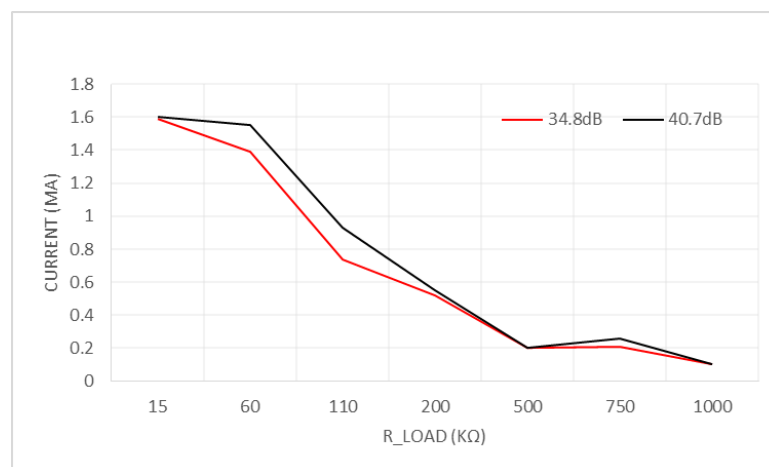
FIGURE 4.12: Peak Current vs R_load

Using a $0 - 2M\Omega$ potentiometer with 20% tolerance, the output voltage on the piezo driver was measured when the hardware boost voltage is set to 105 V. The software gain was then set to 34.8dB and 40.7dB in the software which resulted to the graph in Figure 4.11. As expected, the current also decreases with resistance increasing. These measurements correspond to the peak values in the square wave signals; thus, the effective stimulation values could be represented by average current applied to the skin. The pulses are dependent to the duty cycle of the signal and the time when the stimulation is on. If the stimulation is on for 100ms and the stimulation period is 1Hz, and within the stimulation is a 50% duty cycle of 250 Hz signal, then the effective strength of the signal reduced to $\sim 5\%$.

4.2.1 Hardware Platform

The project involves the development of a hardware device designed to meet the functional requirements outlined. Several sensors, microprocessor, and storage are embedded in the device. A photo of the prototype with the corresponding labels is shown in Figure 4.13. The power supply IC, at the bottom of the PCB, manages the power supply for the board and charging of the battery. The display and WiFi modules are connected using the through-hole connectors. Similarly, there are three electrodes for common, stimulation, and measurement. Furthermore, other peripheral embedded to the board are accelerometer, ADC,RTC and SD module. The microcontroller is programmed and debugged through the JTAG connector. Also note that the PPG sensor and one temperature sensor is in a separate board, since they will have direct contact with the skin. One temperature sensor is on the main board to measure the ambient temperature.
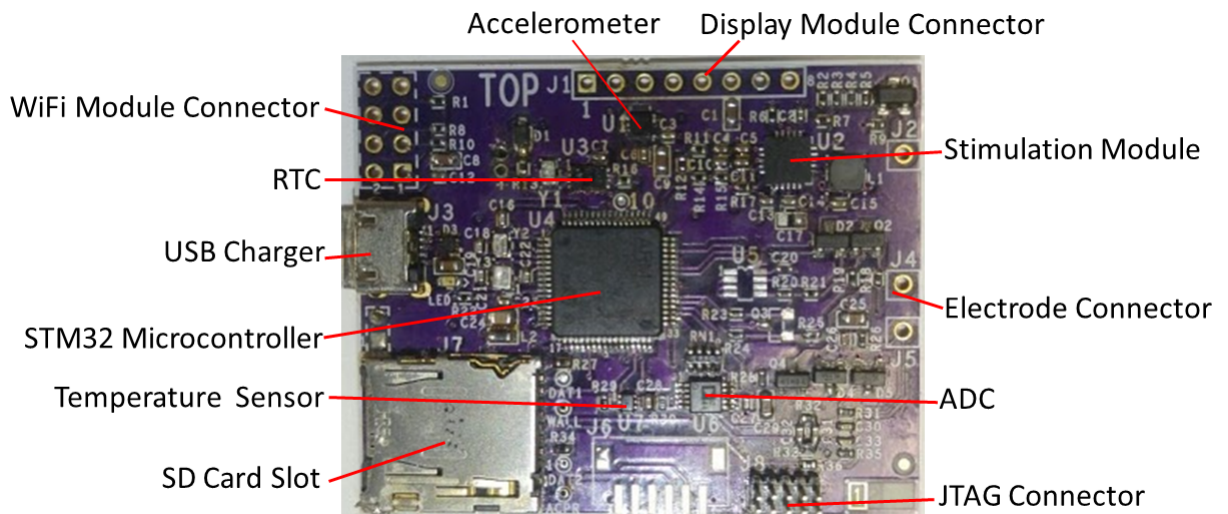
FIGURE 4.13: PCB and Component Layout

Chapter 5

Conclusion and Future Scope

The design of a multi-sensor platform to detect slow wave sleep stage and a sub-threshold electrocutaneous stimulation is presented in this paper. Slow wave sleep is characterized by synchronized low frequency oscillations of brain waves. Due to inaccessible PSG in acquiring accurate sleep data, a wearable device which allows regular data collection is more feasible. The different physiological signals, such as heart rate, EDA, skin temperature and body movement, that contribute to sleep staging are presented; and as a result, sensors as well as circuit configurations were designed for data collection. The sensors were evaluated for performance, cost, power consumption and footprint.

From the experiments conducted, the heart rate data from PPG sensor needs further processing to remove movement artefacts. The heart rate calculation is currently inaccurate due to this noise; however, the presence of movement artefact suggests that the subject is not in SWS stage. If below 40 bpm is considered as invalid heart rate, then the error in the collected data is 1.71%. An accurate representation of measurement error is when a calibrated heart rate measurement system is used for comparison. Next, the actigraphy data from the accelerometer was analyzed. It was seen that calculating the angle with respect to the direction perpendicular to the skin gives a more distinct feature compared to magnitude. Furthermore, the skin and ambient temperature measurements do not provide an

51

accurate measurement of body temperature. The difference between the two readings is insignificant at 0.12% maximum percent difference; thus, one temperature sensor is sufficient for the next design. For the EDA measurements, the simulation and some measurements were shown using a constant voltage reference and 24-bit ADC. It provides wide range of measurement and accuracy from the 24-bit resolution. However, the ADC only provide 22 bit effective resolution at the update rate chose, which leads to an error in measurement by 2 bits. Lastly, using current source and voltage source for skin stimulation was presented and analyzed. It was found the the voltage boost/driver provides flexibility and control to more parameters. The error in measurement of output voltage and current of the stimulation driver is caused by the high tolerance of 20% of the potentiometer used in the experiment. This circuit is not tested with human being; so a more in-depth experiment is required.

A printed circuit board was fabricated for the first prototype of the device. Firmware for the prototype device is developed as a part of this platform. Further analysis of the sleep data collected will be a part of the future scope. For a better quality of signal, it would be helpful to remove movement artefacts; but not necessary since this is an indication that the subject is not in SWS. A complex data fusion algorithm for accurate sleep staging needs to be developed. An updated device prototype integrating the results of this study also needs to be designed to be used in clinical trials.

Appendix A

Market Study on Portable Sleep Monitoring Devices

Brand & Model	Price	Sleep Tracking	Sensors and Hardware	Connectivity	Compatible Platforms	Comments
Microsoft Band (1 & 2)	$250	Yes (Wake, Light Sleep, Deep Sleep)	Galvanic Skin Resistance (GSR sensor), UV sensor, Ambient light sensor, Optical Heart Rate Monitor, Accelerometer/gyrometer, microphone, GPS Display screen	Bluetooth 4.0	Microsoft Health App (supports IOS 7.1 and up, Android 4.2 and up, Windows Phone 8.1)	Has three main sizes (S,M,L) made with hard plastic to keep a snug fit. May get uncomfortable. The screen is helpful.
Jawbone UP3	$199	Yes (Awake, REM, Light, Deep) Equipped with Smart Alarm feature	GSR , body temperature, heart rate, respiration rate sensor, accelerometer (parameters used for sleep staging) No Display screen	Bluetooth 4.0	Up by Jawbone (supports IOS and Android devices only)	Has Smart Coach that acts like a personal trainer. Relatively comfortable fit
Fitbit One	$119	Yes (Awake, Slightly Awake, Asleep)	Accelerometer, altimeter	Bluetooth 4.0	IOS, Android and Windows	Has a separate wristband to install the device on during sleep
Brand & Model	Price	Sleep Tracking	Sensors and Hardware	Connectivity	Compatible Platforms	Comments
Nike Fuelband	$260	No	Accelerometer, ambient light sensor	Bluetooth 4.0	IOS, Android	Mostly just for sports and activity tracking
Asmart Smart Wristband	$20	Yes	No info online	Bluetooth	Zeroner app IOS, Android	Very cheap compared to other brands Detachable USB like device for charging
Avantek Wireless Activity and Sleep Tracker	$129	Yes (Awake, Extremely light, light, deep)	No info online	Bluetooth 4.0	IOS 7 and up only	Claims to track sleep pattern to plan for more restful sleep
Forestfish Smart Bracelet	$49	Yes	Accelerometer	Bluetooth 4.0	IOS and Android	The device is also detachable from the wristband and charges like a USB
Brand & Model	Price	Sleep Tracking	Sensors and Hardware	Connectivity	Compatible Platforms	Comments
Xiaomi Mi Band	$19	Yes (Automatic Sleep Monitoring) (Light and Deep Sleep)	Motion sensor and heart rate	Bluetooth 4.0	Mi band IOS and Android	A very inexpensive device that claims to have a lot of feature Detachable wristband
Zeo Sleep Manager Pro Headband	$99	Yes (Wake, REM, Light and Deep)	EEG electrodes	Bluetooth 4.0	Zeo Mobile Pro App IOS and Android	Has SmartWake alarm technology that wakes the user up at an optimal time
LOHOME Snore Stop BioSensor	$38	No	Infrared Biosensor that detects when the user is snoring	No	N/A	Has mild electrostimulation acupuncture massage to stop the user from snoring
Pivotal Living Tracker 2nd Gen	$49	Yes	3-axis sensor (accelerometer)	Bluetooth 4.0	Pivotal Living IOS and Android	The app doesn't differentiate between sleep stages, but only plots sleep quality

FIGURE A.1: Market Study Results

Appendix B

Component Selection Report

Component	Manufacturer	Man. Part Number	Interface	Package Type	Power Consumption	Eval Board	Price	Comments (FD)
Wifi	Qualcomm	QCA4010/12	I2C, UART, SPI, SDIO	9x9 mm BGA	Low power modes (exact number not on datasheets)	SX-ULPGN-EVK	USD 49.95	Compared to ATWINC1500, it has less community support and is relatively new. PCB footprint is around the same. QCA4012 is dual band - 2.4 and 5GHz (no stock atm)
	Econais	EC19D01	SPI,USART, I2S, SDIO	8x8 mm	RX 40 mA TX 220 mA Shutdown 12.3 uA Idle 1.8 mA	483-1010-ND	CAD 31.95	Dev kit is still available on Digikey but is on obsolete status
	Atmel	ATWINC1500-MR210PA	SPI, UART	22x15mm (w/antenna)	At 19.5 dBm: TX 294 mA, RX 52.5mA , Ivddio 22mA Power Save Modes – 4µA Deep Power Down mode typical @3.3V I/O – 850µA Doze mode			Currently used
	LSR	TiWi-C-W	UART	10.5x10.5 x 1.35 mm	TX Max 360 mA RX 65 mA			Available accessories for antennas are not incorporated in board. No power management feature
	ST	SPWF01SA, SPWF01SC	UART	8X6 mm ECOPACK	Advanced low-power modes – Standby with RTC: 43 µA – Sleep connected (DTIM=1): 15 mA – RX traffic: 105 mA typical	WiFi 4 click	USD 49.00	
		ESP8226	SPI, UART	5x5 mm	-TX CCK at 19.5dBm : 215 mA -RX: 60 mA -Standby: 0.9 mA -Deep Sleep: 10 uA - Power Save: 1.2 mA	WiFi3 Click	USD 27.00	Note: External antenna can be added (i.e. antenova)
Memory	ISSI	IS25LP128	SPI	JM =16-pin SOIC 300mil - JB = 8-pin SOIC 208mil - JF = 8-pin VSOP 208mil	Single 2.3V to 3.6V Voltage Supply - 10 mA Active Read Current - 5 µA Standby Current - Deep Power Down	Flash 3 Click	USD 12.00	
	Atmel	AT24CM02	I2C	–8-lead JEDEC SOIC and Thin or Standard Thickness 8-ball WLCSP	Vcc 1.8V at 400kHz -0.5 mA read Icc -3 mA write Icc -1uA standby current -3uA input and output leakage current	EEPROM 3 c	USD 14.00	
Inertial Measurement Unit (IMU)	Analog Devices	ADXL362	SPI	CC-16-4 , 16-LGA 3 mm × 3.25 mm × 1.06 mm	Ultralow power Power can be derived from coin cell battery -1.8 µA at 100 Hz ODR, 2.0 V supply -3.0 µA at 400 Hz ODR, 2.0	Shake2Wake click	USD 39.00	accel only
	ST	L3GD20	I2C, SPI	LGA 16 4X4X1 mm	Vdd= 3V 6.1 mA supply current -2mA sleep mode -5uA power down	Gyro Click	USD 25.00	gyro only
	ST	LSM6DS3H	I2C, SPI	LGA-14L 2.5 X 3 X 0.83 mm	0.85 mA in combo normal mode and 1.1 mA in combo high-performance mode up to 1.6 kHz	STEVAL-MKI128V5	CAD 15.00	HTS221, LIS3MDL, LPS22HB, LSM6DS3H, UVIS25 - Accelerometer, Gyroscope, Humidity, Magnetometer, Pressure, Temperature Sensor Evaluation Board
Battery Charger and Power Management Chip	Linear Technology	LTC3586	-	38-pin 4mm × 6mm QFN package	<30µA No-Load Quiescent Current when Powered from BAT			MikroE Click 2 uses this chip
Isolation	Analog Devices	AD202	-	SIP Package 52.8x2.5x6.3 mm	35mW (AD204) and 75mW(AD202)			Something to consider for protection in data collection

Appendix C

Power Consumption Calculation

Sonya Power Consumption EstimatorTemplate   Prepared by: Francia Dauz
Note: Change values in orange cells

Modules/ Peripherals	Vdd	Configuration	Current Consumption	Power Consumption	Time (24hr)	Average Current
STM32L4 MCU at 25MHz	3.3	Active/Run(all peripherals enabled)	35 mA	115.5 mW	8	16.35 mA
		Sleep	28 mA	92.4 mW	4	
		Standby	0.036 mA	0.1188 mW	12	
		Wake Up(from standby mode) 0.48ms	8.4 mA	27.72 mW		
		Wake Up(from sleep mode) 5cpuclockcycle	1.7 mA	5.61 mW		
Heart Rate Monitor	1.8	Active/Run	1.2 mA	2.16 mW	8	0.47 mA
		Sleep	0.1 mA	0.18 mW	16	
		IR LED	20 mA	6.5 mW	0	
		RED LED	20 mA	9.8 mW	0	
Accelerometer	3.3	Active/Run	0.594 mA	1.9602 mW	8	0.21 mA
		Sleep	0.0165 mA	0.05445 mW	16	
RTC	3.3	Active/Run (Timekeeping)	0.0012 mA	0.00396 mW	24	0.02 mA
		Sleep	0.001 mA	0.0033 mW		
		Read	0.3 mA	0.99 mW	0.5	
		Write	0.4 mA	1.32 mW	0.5	
Temperature (x2)	3.3	Active/Run	0.015 mA	0.0495 mW	8	0.01 mA
		Sleep	0.01 mA	0.033 mW	16	
Display	3.3	Active/Run (Logic)	0.3 mA	0.99 mW	23	7.80 mA
	7.5	Display Power (50% Display Area ON)	21.6 mA	162 mW	1	
AD7791	3.3	Active/Run	0.075 mA	0.2475 mW	8	0.03 mA
		Sleep	0.001 mA	0.0033 mW	16	
SD Card (refer swissbit uSD)	3.3	Read	30 mA	99 mW	1	2.92 mA
		Write	40 mA	132 mW	1	
ESP8226 TX/RX	3.3	Average Current	80 mA	264 mW		
		at 19.5 dBm TX	215 mA	709.5 mW	1	12.56 mA
		RX	60 mA	198 mW	1	
		Standby	0.9 mA	2.97 mW		
		Deep Sleep	0.01 mA	0.033 mW		
		Power Save	1.2 mA	3.96 mW	22	
		Shutdown	0.0005 mA	0.00165 mW		

Total Current Consumption	40.37 mA	per hour
	968.788 mA	per day

If Target Battery Life given	1200 hr	50 days
Battery Capacity Required	48439.4 mAh	

If Battery capacity given	800 mAh
Battery life	19.8186 hours

Appendix D
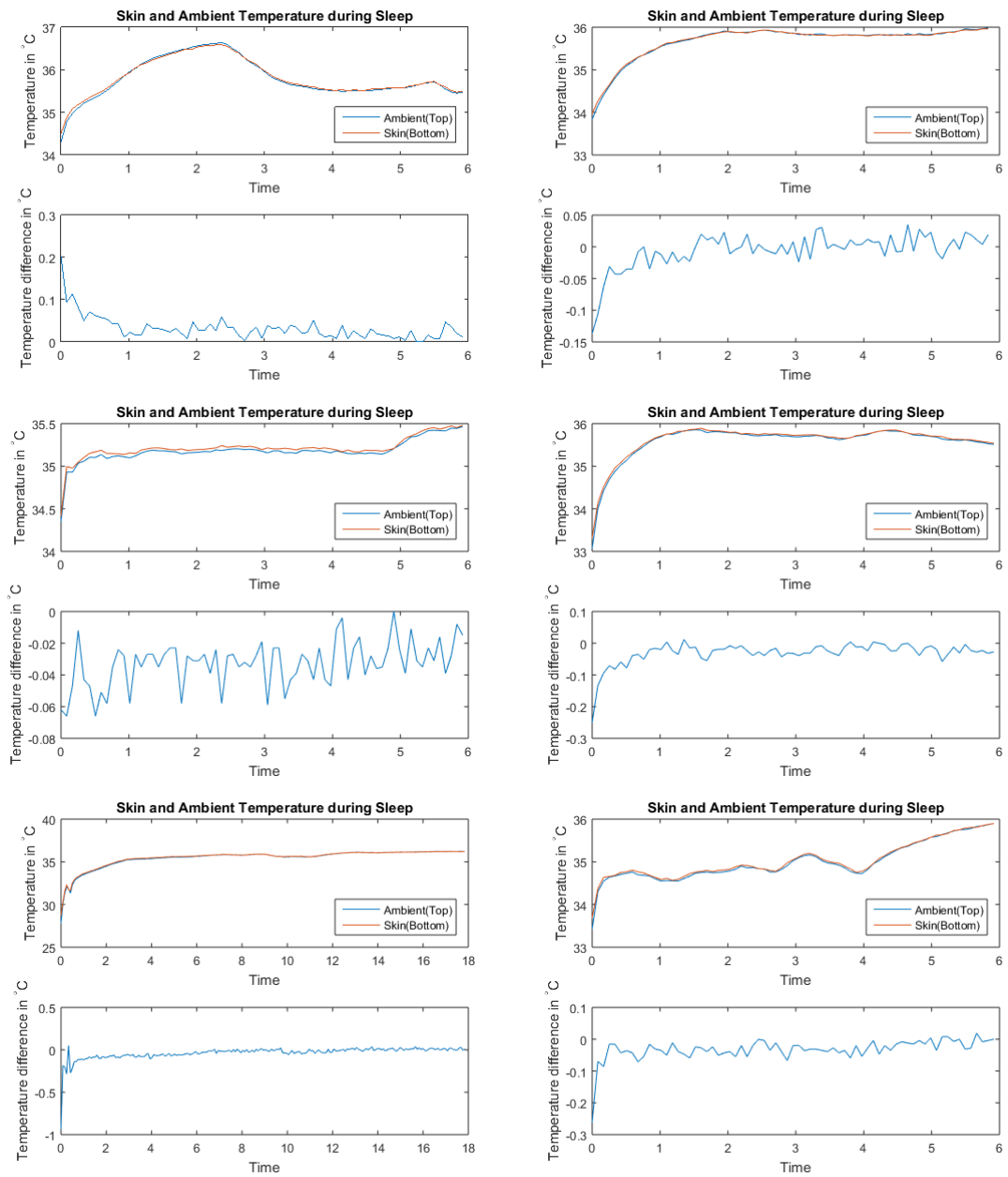
Skin and Ambient Temperature plots for Six Nights

FIGURE D.1: Skin vs Ambient Temperature Comparison

Bibliography

[1] M. Hafner, M. Stepanek, J. Taylor, W. M. Troxel, and C. van Stolk, "Why sleep matters–the economic costs of insufficient sleep," 2016.

[2] G. Garcia-Molina, F. Abtahi, and M. Lagares-Lemos, "Automated NREM sleep staging using the Electro-oculogram: A pilot study," in *2012 Annual International Conference of the IEEE Engineering in Medicine and Biology Society (EMBC)*, pp. 2255–2258, Aug. 2012.

[3] R. B. Berry *et al.*, "The aasm manual for the scoring of sleep and associated events," *Rules, Terminology and Technical Specifications, Darien, Illinois, American Academy of Sleep Medicine*, 2012.

[4] T. Kanda *et al.*, "Sleep as a biological problem: an overview of frontiers in sleep research," *The Journal of Physiological Sciences*, vol. 66, no. 1, pp. 1–13, 2016.

[5] B. Rasch and J. Born, "About sleep's role in memory," *Physiological reviews*, vol. 93, no. 2, pp. 681–766, 2013.

[6] M. Walker, "The role of slow wave sleep in memory processing," *Journal of Clinical Sleep Medicine Supplement to Vol*, vol. 5, no. 2, p. S20, 2009.

[7] J. D. Feusner *et al.*, "Effects of cranial electrotherapy stimulation on resting state brain activity," *Brain and behavior*, vol. 2, no. 3, pp. 211–220, 2012.

[8] P. A. Indursky, V. V. Markelov, V. M. Shakhnarovich, and V. B. Dorokhov, "Low-frequency rhythmic electrocutaneous hand stimulation during

slow-wave night sleep: Physiological and therapeutic effects," *Human Physiology*, vol. 39, pp. 642–654, Nov 2013.

[9] K. A. I. Aboalayon, H. T. Ocbagabir, and M. Faezipour, "Efficient sleep stage classification based on EEG signals," in *Systems, Applications and Technology Conference (LISAT), 2014 IEEE Long Island*, pp. 1–6, May 2014.

[10] Y. H. Lee, Y. S. Chen, and L. F. Chen, "Automated Sleep Staging Using Single EEG Channel for REM Sleep Deprivation," in *Ninth IEEE International Conference on Bioinformatics and BioEngineering, 2009. BIBE '09*, pp. 439–442, June 2009.

[11] M. Radha, G. Garcia-Molina, M. Poel, and G. Tononi, "Comparison of feature and classifier algorithms for online automatic sleep staging based on a single EEG signal," in *2014 36th Annual International Conference of the IEEE Engineering in Medicine and Biology Society (EMBC)*, pp. 1876–1880, Aug. 2014.

[12] A. J. Casson, D. C. Yates, S. J. M. Smith, J. S. Duncan, and E. Rodriguez-Villegas, "Wearable Electroencephalography," *IEEE Engineering in Medicine and Biology Magazine*, vol. 29, pp. 44–56, May 2010.

[13] J. D. Geyer, S. Talathi, and P. R. Carney, "Introduction to sleep and polysomnography," *Reading EEGs: a practical approach, Lippincott Williams & Wilkins, Philadelphia*, 2009.

[14] P. Silapachote, A. Srisuphab, T. Bhunnachet, and N. Matrakool, "A miniature home-based sleep monitoring device," in *TENCON 2015 - 2015 IEEE Region 10 Conference*, pp. 1–5, Nov. 2015.

[15] S. F. Liang, C. P. Young, D. W. Chang, F. Z. Shaw, Y. D. Liu, Y. C. Liu, and J. J. Chen, "Development of an actigraph system for sleep-wake identification," in *2011 IEEE Instrumentation and Measurement Technology Conference (I2MTC)*, pp. 1–6, May 2011.

[16] Y. T. Peng, C. Y. Lin, M. T. Sun, and C. A. Landis, "Multimodality Sensor System for Long-Term Sleep Quality Monitoring," *IEEE Transactions on Biomedical Circuits and Systems*, vol. 1, pp. 217–227, Sept. 2007.

[17] C. T. Fan, Y.-K. Wang, and J.-R. Chen, "Home sleep care with video analysis and its application in smart TV," in *2014 IEEE 3rd Global Conference on Consumer Electronics (GCCE)*, pp. 42–43, Oct. 2014.

[18] A. Heinrich, X. Aubert, and G. d. Haan, "Body movement analysis during sleep based on video motion estimation," in *2013 IEEE 15th International Conference on e-Health Networking, Applications Services (Healthcom)*, pp. 539–543, Oct. 2013.

[19] V. Verhaert, B. Haex, T. D. Wilde, D. Berckmans, M. Vandekerckhove, J. Verbraecken, and J. V. Sloten, "Unobtrusive Assessment of Motor Patterns During Sleep Based on Mattress Indentation Measurements," *IEEE Transactions on Information Technology in Biomedicine*, vol. 15, pp. 787–794, Sept. 2011.

[20] L. Samy, M. C. Huang, J. J. Liu, W. Xu, and M. Sarrafzadeh, "Unobtrusive Sleep Stage Identification Using a Pressure-Sensitive Bed Sheet," *IEEE Sensors Journal*, vol. 14, pp. 2092–2101, July 2014.

[21] R. Liguori *et al.*, "Sleep stage-related changes in sympathetic sudomotor and vasomotor skin responses in man," *Clinical Neurophysiology*, vol. 111, pp. 434–439, Mar. 2000.

[22] A. Sano, R. W. Picard, and R. Stickgold, "Quantitative analysis of wrist electrodermal activity during sleep," *Int J Psychophysiol*, vol. 94, pp. 382–389, Dec. 2014.

[23] S. H. Hwang, S. Seo, H. N. Yoon, D. W. Jung, H. J. Baek, J. Cho, J. W. Choi, Y. J. Lee, D. U. Jeong, and K. S. Park, "Sleep Period Time Estimation Based on Electrodermal Activity," *IEEE Journal of Biomedical and Health Informatics*, vol. PP, no. 99, pp. 1–1, 2015.

[24] J. J. Braithwaite, D. G. Watson, R. Jones, and M. Rowe, "A guide for analysing electrodermal activity (eda) & skin conductance responses (scrs) for psychological experiments," *Psychophysiology*, vol. 49, pp. 1017–1034.

[25] A. M. Bianchi, M. O. Mendez, and S. Cerutti, "Processing of Signals Recorded Through Smart Devices: Sleep-Quality Assessment," *IEEE Transactions on Information Technology in Biomedicine*, vol. 14, pp. 741–747, May 2010.

[26] S. Sangurmath and N. Daimiwal, "Application of photoplethysmography in blood flow measurement," in *2015 International Conference on Industrial Instrumentation and Control (ICIC)*, May 2015.

[27] M. K. Uçar, M. R. Bozkurt, K. Polat, and C. Bilgin, "Investigation of effects of time domain features of the photoplethysmography (PPG) signal on sleep respiratory arrests," in *Signal Processing and Communications Applications Conference (SIU), 2015 23th*, pp. 124–127, May 2015.

[28] I. Hermawan, M. S. Alvissalim, M. I. Tawakal, and W. Jatmiko, "An integrated sleep stage classification device based on electrocardiograph signal," in *2012 International Conference on Advanced Computer Science and Information Systems (ICACSIS)*, pp. 37–41, Dec. 2012.

[29] Y. Chen, X. Zhu, and W. Chen, "Automatic sleep staging based on ECG signals using hidden Markov models," in *2015 37th Annual International Conference of the IEEE Engineering in Medicine and Biology Society (EMBC)*, pp. 530–533, Aug. 2015.

[30] J.-S. Wang, G.-R. Shih, and W.-C. Chiang, "Sleep stage classification of sleep apnea patients using decision-tree-based support vector machines based on ECG parameters," in *2012 IEEE-EMBS International Conference on Biomedical and Health Informatics (BHI)*, pp. 285–288, Jan. 2012.

[31] A. Klein, O. R. Velicu, N. M. Madrid, and R. Seepold, "Sleep stages classification using vital signals recordings," in *2015 12th International*

Workshop on Intelligent Solutions in Embedded Systems (WISES), pp. 47–50, Oct. 2015.

[32] H. Abdullah, N. Maddage, I. Cosic, and D. Cvetkovic, "Brain and heart interaction during sleep in the healthy and sleep apnoea," in *2010 IEEE EMBS Conference on Biomedical Engineering and Sciences (IECBES)*, pp. 276–280, Nov. 2010.

[33] R. Ferber, R. Millman, M. Coppola, J. Fleetham, C. F. Murray, C. Iber, V. McCall, G. Nino-Murcia, M. Pressman, and M. Sanders, "Portable recording in the assessment of obstructive sleep apnea. asda standards of practice.," *Sleep*, vol. 17, no. 4, pp. 378–392, 1994.

[34] B. Zoefel, R. J. Huster, and C. S. Herrmann, "Neurofeedback training of the upper alpha frequency band in EEG improves cognitive performance," *NeuroImage*, vol. 54, pp. 1427–1431, Jan. 2011.

[35] M. A. Nitsche *et al.*, "Transcranial direct current stimulation: State of the art 2008," *Brain Stimulation*, vol. 1, pp. 206–223, July 2008.

[36] B. Stinson and D. Arthur, "A novel EEG for alpha brain state training, neurobiofeedback and behavior change," *Complementary Therapies in Clinical Practice*, vol. 19, pp. 114–118, Aug. 2013.

[37] S.-H. Jin *et al.*, "Nonlinear dynamics of the EEG separated by independent component analysis after sound and light stimulation," *Biological Cybernetics*, vol. 86, p. 395, May 2002.

[38] Y. V. Gulyaev, A. S. Bugaev, P. A. Indursky, V. M. Shakhnarovich, and V. V. Dementienko, "Improvement of the night sleep quality by electrocutaneous subthreshold stimulation synchronized with the slow wave sleep," *Doklady Biological Sciences*, vol. 474, pp. 132–134, May 2017.

[39] U. F. Pliquett and C. A. Gusbeth, "Perturbation of human skin due to application of high voltage," *Bioelectrochemistry*, vol. 51, no. 1, pp. 41 – 51, 2000.

[40] S. F. Cogan, K. A. Ludwig, C. G. Welle, and P. Takmakov, "Tissue damage thresholds during therapeutic electrical stimulation," *Journal of neural engineering*, vol. 13, no. 2, p. 021001, 2016.

[41] J. L. Mason and N. A. MacKay, "Pain sensations associated with electrocutaneous stimulation," *IEEE Transactions on Biomedical Engineering*, no. 5, pp. 405–409, 1976.

[42] "A 75 W Real-Time Scalable Body Area Network Controller and a 25 W ExG Sensor IC for Compact Sleep Monitoring Applications," vol. 47.

Vita Auctoris

Name: Francia Tephanie Dauz

Education:

- University of Windsor, B.A.Sc. Electrical Engineering

- University of WIndsor, M.A.Sc. Electrical Engineering